JCI The Journal of Clinical Investigation

Cathelicidin antimicrobial peptide expression in neutrophils and neurons antagonistically modulates neuroinflammation

Subash Chand Verma, … , Roland Liblau, Julien Diana

J Clin Invest. 2024. https://doi.org/10.1172/JCI184502.

Research In-Press Preview Autoimmunity Immunology

Graphical abstract

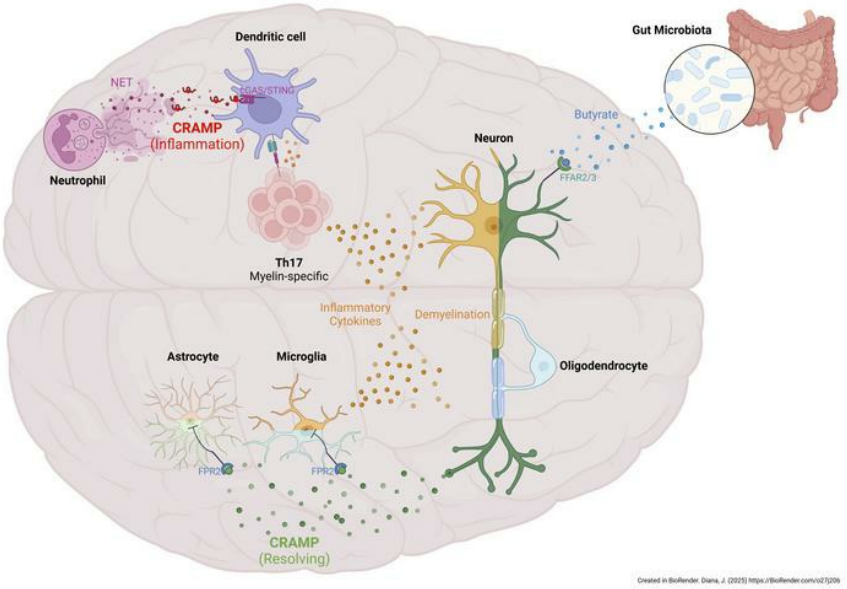

Cathelicidin antimicrobial peptide expression in neutrophils and neurons antagonistically modulates neuroinflammation.

Subash Chand Verma[1*], Emmanuelle Enée[1*], Kanchanadevi Manasse[1], Feriel Rebhi[1], Axelle Penc[1], David Romeo-Guitart[1], Cuc Bui Thi[1], Matthias Titeux[2], Franck Oury[1], Simon Fillatreau[1,3], Roland Liblau[4,5], Julien Diana[1].

[1]Université Paris Cité, CNRS, INSERM, Institut Necker Enfants Malades-INEM, F-75015 Paris, France.

[2]Université Paris Cité, Imagine Institute, INSERM U1163, 75015 Paris, France.

[3]APHP, Hôpital Necker-Enfants Malades, F-75015 Paris, France.

[4]Toulouse Institute for Infectious and Inflammatory Diseases (Infinity), CNRS, INSERM, Université Paul-Sabatier de Toulouse (UPS), Toulouse, France.

[5]Department of Immunology, Toulouse University Hospital, Toulouse, France.

*: co-authors.

Running title: Dual role of cathelicidin in neuroinflammation.

Corresponding Author: Julien Diana, Institut Necker Enfants Malades (INEM), 160 rue de Vaugirard, 75015 Paris, France ; Phone : + 33140615385 ; E-mail: julien.diana@inserm.fr

Keywords: neuroinflammation; autoimmunity; antimicrobial peptides; multiple sclerosis.

Abstract

Multiple sclerosis (MS) is an autoimmune disease that affects the central nervous system (CNS), the pathophysiology of which remains unclear and for which there is no definitive cure. Antimicrobial peptides (AMPs) are immunomodulatory molecules expressed in various tissues, including the CNS. Here, we investigated whether the cathelicidin-related AMP (CRAMP) modulated the development of experimental autoimmune encephalomyelitis (EAE), a mouse model of MS. We showed that, at early stage, CNS-recruited neutrophils produced neutrophil extracellular traps (NETs) rich in CRAMP that was required for EAE initiation. NET-associated CRAMP stimulated IL-6 production by dendritic cells via the cGAS/STING pathway, thereby promoting encephalitogenic Th17 response. However, at a later disease stage, neurons also expressed CRAMP that reduced EAE severity. *Camp* knockdown in neurons led to disease exacerbation, while local injection of $CRAMP_{1-39}$ at the peak of EAE promoted disease remission. In vitro, $CRAMP_{1-39}$ regulated the activation of microglia and astrocytes through the formyl peptide receptor (FPR)2. Finally, administration of butyrate, a gut microbiota-derived metabolite, stimulated the expression of neural CRAMP via the free fatty acids receptors (FFAR)2/3, and prevented EAE. This study shows that CRAMP produced by different cell types have opposing effects on neuroinflammation, offering therapeutic opportunities for MS and other neuroinflammatory disorders.

Introduction

Multiple sclerosis (MS) is an autoimmune disease that affects the central nervous system (CNS) and exhibits increasing incidence. The hallmarks of MS include CNS infiltration by immune cells, activation of glial cells, multifocal demyelination, and axonal loss. The disease is influenced by multiple genetic polymorphisms and environmental factors including the intestinal microbiota that is thought to play a critical role in the development of the disease (1, 2). There is still no satisfying therapy for MS (3).

A better understanding of the immune processes at play in MS has been achieved using the pre-clinical model experimental autoimmune encephalomyelitis (EAE) (4). EAE can be induced by immunization with various myelin antigens such as myelin oligodendrocyte glycoprotein (MOG) activating self-reactive $CD4^+$ T helper (Th) 1 and 17 cells. Upon migration to the CNS, T cells initiate a local inflammatory response leading to axonal demyelination (5). Innate immune cells such as microglia, dendritic cells, and macrophages play a critical role in this local inflammatory response (6, 7).

The relevance of antimicrobial peptides (AMPs) in autoimmunity is increasingly acknowledged. AMPs were discovered more than 40 years ago and represent a crucial component of the innate immune system in all living organisms (8). They are mainly produced at epithelial surfaces and protect against invading microorganisms while maintaining the homeostasis of the commensal microbiota (9, 10). AMPs also have important immunomodulatory roles and can be either pro- or anti-inflammatory depending on the context (11). For instance, AMPs play a role in the immunopathogenesis of various autoimmune diseases. AMPs from activated neutrophils can bind various toll-like receptor (TLR) ligands and activate the immune system contributing to the initiation of autoimmunity (12). A mechanism common to many autoimmune and autoinflammatory diseases is the ability of cathelicidin from neutrophil extracellular traps (NETs), complexed with nucleic acids, to induce

inflammatory cytokines from myeloid cells (13-15). In contrast, AMPs secreted by non-immune cells can prevent autoimmune responses by inducing various regulatory immune cell types including regulatory macrophages and B cells by engaging their receptors at the surface of these cells (16).

Emerging evidence suggests that AMPs are a part of the immune defense of the CNS (17, 18). AMPs are expressed in the CNS of rodents and humans at a steady state, and their expression increases in the context of infection (19-23). Following bacterial infection, CRAMP is expressed in the CNS by recruited neutrophils, as well as by activated astrocytes, microglia, and meningeal cells (21, 24). In an experimental model of pneumococcal meningitis, mice deficient in CRAMP showed a higher degree of glial cell activation and CNS inflammation (25, 26).

In this study, we investigated whether CRAMP is expressed in the CNS during the development of EAE and plays a critical role in controlling neuroinflammation.

Results

CRAMP shows opposite roles during EAE. As a starting point, we evaluated the expression of CRAMP in the CNS during the development of EAE in C57BL/6 wild-type (WT) mice. The mRNA expression of *Camp*, encoding for CRAMP, increased in spinal cord (SC) during the course of EAE, peaking 12 days after immunization (Figure 1A). We observe that complete Freund's adjuvant (CFA) was sufficient to induce *Camp* mRNA expression in the CNS suggesting that peripheral inflammation can trigger *Camp* expression in the CNS (Supplemental Figure 1). Importantly, CRAMP-deficient *Camp*$^{-/-}$ C57BL/6 mice exhibited significantly reduced EAE scores (Figure 1B), indicating that the expression of CRAMP was necessary for EAE development. To determine whether the absence of CRAMP prevented the initiation of the encephalitogenic T cell response in the periphery, we analyzed Myelin Oligodendrocyte Glycoprotein (MOG)$_{35-55}$-specific CD4$^+$ T cells using MOG$_{35-55}$/IAb tetramer staining. Seven days after immunization, the frequency of MOG$_{35-55}$-specific CD4$^+$ T cells in the draining lymph nodes (dLNs) was comparable between WT and *Camp*$^{-/-}$ mice, indicating that CRAMP did not play a role in the priming of autoreactive T cells in the periphery (Figure 1C). To confirm the ability of *Camp*$^{-/-}$ mice to mount an effective immune response, we immunized them with ovalbumin (OVA) and transferred CFSE-labeled OVA-specific CD4$^+$ OT-II T cells. Five days after, analyzing OT-II T cell proliferation in the dLNs, we observed similar proliferation regardless of *Camp* deficiency (Supplemental Figure 2). Further supporting that CRAMP was not required for the initiation of the T cell response, twelve days after immunization, the frequency and number of MOG$_{35-55}$-specific CD4$^+$ T cells in the SC were similar between WT and *Camp*$^{-/-}$ mice (Figure 1D). However, the expression of IL-17 and IFNγ in CD4$^+$ T cells were reduced in *Camp*$^{-/-}$ mice supporting a local control of the encephalitogenic T cell response by CRAMP in CNS (Figure 1E). These data underline a role for CRAMP in the promotion of the pathogenic autoreactive CD4$^+$ T cell response in the CNS.

To further define the role of CRAMP in EAE, we injected recombinant $CRAMP_{1-39}$ peptide intraperitoneally (i.p.) in WT mice before the symptomatic phase (day 7) or at the peak of the disease (day 15). Surprisingly, the presymptomatic treatment reduced the severity of EAE, and therapeutic treatment at day 15 promoted EAE remission (Figure 1, F-G). Biodistribution experiments showed that Cy5-labeled $CRAMP_{1-39}$ localized to the brain and SC 30 min after i.p. injection and remained at these sites for at least 24 h (Supplemental Figure 3). Similarly, local administration of $CRAMP_{1-39}$ within the intrathecal (i.t.) space of the spine 9 days after EAE induction resulted in a comparable beneficial outcome (Figure 1H). The expression of neurofilament light chain (NF-L) protein in the serum of i.t. $CRAMP_{1-39}$-treated mice on day 15 was decreased compared to untreated mice, indicating a reduced neuronal damage (Figure 1I). In addition, i.t. $CRAMP_{1-39}$ treatment decreased the activation of astrocytes and microglia in the SC as shown by decreased expression of CD44 and CD86, respectively (Figure 1, J-K). The data obtained with $CRAMP_{1-39}$ peptide administration suggest that this AMPs also has protective role in EAE. We conclude that CRAMP might have antagonistic functions in EAE, and proceeded with the investigation of these effects.

CRAMP is expressed in different cell types within the CNS during EAE. We envisioned that the opposite effects of CRAMP in EAE might relate to its expression in different cell types. We thus analyzed the expression of CRAMP in the CNS at the peak of EAE using confocal microscopy. CRAMP was expressed in SC by $MAP2^+$ neurons and minimally by $GFAP^+$ astrocytes, but predominantly by $MAP2^-$ $GFAP^-$ cells (Figure 2A). Neuronal expression of CRAMP was also observed in the NSC-34 motor neuron-like cells (Figure 2B and Supplemental Figure 4A). CRAMP staining colocalized with Synaptophysin, a marker of presynaptic vesicles, suggesting that CRAMP can be actively secreted by neurons. It is known that neutrophils infiltrate the CNS early during EAE (27). By confocal microscopy we

confirmed the massive infiltration of the SC by neutrophils after EAE induction. The expression of CRAMP by these neutrophils and the presence of NETs were observed in the SC at day 12 and the dLNs at day 7 (Figure 2C and Supplemental Figure 4B, C). By flow cytometry, we confirmed the recruitment of CRAMP-expressing activated neutrophils ($CD62L^{low}$) in the CNS during the initiation of EAE while neutrophils remained non-activated and did not express CRAMP at their surface in the bone marrow (BM) from tibia (Figure 2D). The kinetic of surface CRAMP expression showed high expression in the neutrophils ($CD45^+$ $CD11b^+$ $Ly6G^+$ $Ly6C^{low}$) peaking at day 10, mild expression in neurons ($CD45^-$ $NeuN^+$) and microglia ($CD45^{med}$ $CD11b^+$) peaking at day 15 and low expression in astrocytes ($CD45^-$ $GFAP^+$) peaking at day 15 (Figure 2E). These data showed that CRAMP was expressed in neutrophils and CNS-resident cells in the CNS during EAE. This was consistent with the hypothesis that the opposite effect of CRAMP on the disease could be explained by different cell sources.

CRAMP from neutrophils is essential for EAE. To determine the functional role of CRAMP produced by neutrophils, we generated mice lacking *Camp* specifically in this cell type (Mrp8-Cre^{Tg}.$Camp^{f/f}$ mice) obtained by crossing Mrp8-Cre^{Tg} and $Camp^{flox/flox}$ C57BL/6 mice (Supplemental Figure 5A–B). We observed that Mrp8-Cre^{Tg}.$Camp^{f/f}$ mice were almost resistant to EAE induction, recapitulating the phenotype observed in germline $Camp^{-/-}$ mice and demonstrating the mandatory role of CRAMP from neutrophils for EAE development (Figure 3A). Flow cytometry analysis of the immune infiltrate in the SC at the peak of the EAE in Mrp8-Cre^{Tg}.$Camp^{f/f}$ and Mrp8-Cre^{neg}.$Camp^{f/f}$ did not reveal significant differences in terms of cell number or cell types including neutrophils (Figure 3B). However, RT-qPCR analysis of the SC showed a reduced expression of the inflammatory cytokines *Ifnγ* and *Il-17*, as well as *Il-6*, in Mrp8-Cre^{Tg}.$Camp^{f/f}$ (Figure 3C). These results suggested a local regulation of disease development that we next confirmed by transfer experiments. Indeed, the transfer of

splenocytes from immunized Mrp8-Cre^{Tg}.*Camp*$^{f/f}$ or Mrp8-Cre^{neg}.*Camp* $^{f/f}$ mice into C57BL/6 mice induced EAE to the same extent (Figure 3D). However, the transfer of splenocytes from immunized C57BL/6 mice induced EAE in Mrp8-Cre^{neg}.*Camp* $^{f/f}$ mice but not as effectively in Mrp8-Cre^{Tg}.*Camp*$^{f/f}$ (Figure 3E), even though the transfer of splenocytes from immunized C57BL/6 CD45.1 mice into Mrp8-Cre^{neg}.*Camp* $^{f/f}$ or Mrp8-Cre^{Tg}.*Camp*$^{f/f}$ mice showed no difference in terms of migration of the transferred T cells into the SC and the brain (Figure 3F). These data supported the notion that CRAMP from neutrophils promoted EAE development locally in the CNS rather than in the periphery.

CRAMP from NETs favors encephalitogenic T cell response. During EAE, we observed infiltration of CRAMP^{+} NETting neutrophils in the CNS (Figure 2B and Supplemental Figure 4B). Previous studies have shown that NETs contribute via various pathways to the pathogenesis of several autoimmune diseases, including CNS pathologies (28-30). To investigate the role of NETs in EAE development, we administrated the pan-peptidylarginine deiminase (PAD) inhibitor Cl-amidine subcutaneously to WT mice to inhibit NET formation during EAE. We observed that blocking NET formation from day 7 to day 17 after EAE induction significantly reduced disease severity (Figure 4A) and the circulating level of NF-L (Figure 4B). Similarly, neutrophil depletion with anti-Ly6G mAb during the same period also resulted in reduced EAE severity (Figure 4C). To determine the direct effect of NETs on encephalitogenic T cell response, we produced and isolated NETs in vitro from WT and *Camp*$^{-/-}$ neutrophils. We observed that WT and *Camp*$^{-/-}$ neutrophils were able to form NETs similarly (Figure 4D). We added NETs to a culture of splenocytes isolated from EAE-immunized WT mice. WT NETs stimulated the expression of IL-6, IL-23 and IL-17 (Figure 4E), consistent with previous reports demonstrating that NETs promote Th17 response (31). However, CRAMP-deficient NETs failed to promote Th17 response when added to splenocytes from

EAE-immunized C57BL/6 mice (Figure 4F). CRAMP is known to promote myeloid immune cell responses to self-nucleic acids released during NETosis by binding and transporting nucleic acids into the cells and enabling their recognition by intracellular sensors such as TLR9, Aim2, or cGAS-STING (15, 32). To confirm this, we generated bone-marrow derived dendritic cells (BMDCs) and stimulated them with NETs in the presence of TDI-6570, a specific cGAS inhibitor, or the ODN A151, a multi-specific TLR9, AIM2 and cGAS antagonist. We observed that NETs stimulated IL-6 from BMDCs and this stimulatory effect was abolished by TDI-6570 and A151 (Figure 4G). Taken together, CRAMP from CNS-infiltrating neutrophils appeared to be a key molecule promoting EAE development by stimulating the local encephalitogenic Th17 response, possibly via the cGAS-STING pathway.

CRAMP from neurons dampens EAE. As we identified CRAMP expression in neurons, we wanted to determine the functional role of this neural CRAMP on EAE development. To achieve this objective, we performed i.t. injection in WT mice with adeno-associated virus serotype 9 (AAV9) expressing *Camp* shRNA or scramble shRNA sequence under the U6 promoter to knockdown of *Camp* expression by neurons (Supplemental Figure 6). AAV9-sh*Camp* were i.t. injected 7 days before EAE induction in order to selectively reach neurons, and not CNS-infiltrating cells. We observed that prophylactic knockdown of *Camp* expression in the SC significantly exacerbated the severity of EAE, supporting a protective role for CRAMP from neurons. (Figure 5A). In addition, the oral treatment of WT mice with butyrate, a gut microbiota-derived short chain fatty acid (SCFA) known to induce cathelicidin in several tissues (33), induced CRAMP expression in the CNS at steady state (Figure 5B) and showed protective effect against EAE (Figure 5C). By cell sorting from the CNS, we observed that while butyrate increased *Camp* expression in neurons, microglia and astrocytes, it decreased *Camp* expression in neutrophils (Supplemental Figure 7A). The protective effect of butyrate

involved CRAMP from neurons since butyrate treatment was less effective at reducing EAE severity in mice pretreated with i.t. AAV9-sh*Camp* while it remained protective in mice treated with AAV9-sh*Scramble* (Figure 5D). Other SCFAs, acetate and propionate, also stimulated CRAMP expression in the CNS after oral administration but not significantly (Supplemental Figure 7B). Finally, in vitro experiments using the NSC-34 neurons, showed that as in vivo, butyrate but not acetate or propionate significantly induced *Camp* expression in neurons. Importantly, using a specific antagonist GLPG 0974, we showed that the stimulatory effect of butyrate on neurons was mediated through the free fatty acid receptor (FFAR)2/3 receptors (Figure 5E).

To molecularly define the regulatory effect of CRAMP on the encephalitogenic response, we added growing dose of $CRAMP_{1-39}$ on splenocyte culture from EAE-immunized WT mice and we observed a significant reduction in a dose-dependent manner of the expression of IL-17, CCL-2 and IL-6 while IFNγ expression was poorly impacted (Figure 5F). Notably, these inhibitory effects were observed when $CRAMP_{1-39}$ was applied at 10 $\mu g.mL^{-1}$, which caused little toxicity in the treated cultures, whereas the expression of all cytokines decreased at the dose of 30 $\mu g.mL^{-1}$, because this high concentration of $CRAMP_{1-39}$ killed all cells (Supplemental Figure 8). Accordingly, the transfer of splenocytes from MOG_{35-55}-immunized C57BL/6 mice cultured in the presence of $CRAMP_{1-39}$ (10 $\mu g.mL^{-1}$) was less efficient at inducing EAE in C57BL/6 mice compared with control splenocytes not exposed to $CRAMP_{1-39}$ (Figure 5G). Together, these data suggested a model where CRAMP from neurons can control the encephalitogenic response locally.

CRAMP dampens microglia and astrocyte activation. IL-6, IL-23 and CCL2 are critical cytokines and chemokines expressed by microglia, the CNS-resident macrophages (34), and known to promote the expansion of encephalitogenic Th17 cells during EAE (35). Cathelicidin

is known to modulate the phenotype of myeloid immune cells as example preventing the activation of macrophages by TLR ligands (36). Therefore, we hypothesized that CRAMP prevented microglial activation during EAE leading to poor Th17 response. To address this question, we isolated primary microglia and cultured them with $CRAMP_{1-39}$. Using microglia from *Camp*$^{-/-}$ mice, we observed that exogenous $CRAMP_{1-39}$ efficiently targeted microglia cells and localized in both their membrane as well as their cytoplasm (Figure 6A). Importantly, $CRAMP_{1-39}$ reduced the production of the pro-Th17 cytokines CCL2, IL-6, and IL-23 by LPS-activated microglia (Figure 6B). By using specific antagonists for receptors known to interact with CRAMP and to be expressed by microglia, we determined that $CRAMP_{1-39}$ mediated its regulatory effect through the formyl peptide receptor 2 (FPR2), rather than the purinergic ionotropic P2X7 receptor (P2X7R) (Figure 6C and supplemental Figure 9A-B). In addition, $CRAMP_{1-39}$ also reduced microglial activation induced by a cocktail of IFNγ and TNFα and this regulatory effect was FPR2-dependent (Supplemental Figure 9C). Using primary astrocyte cultures, we demonstrated a similar ability of $CRAMP_{1-39}$ to target this cell type and to decrease inflammatory cytokine expression (IL-6, TNF-α, CCL2) induced by LPS via FPR2 (Figure 6D-E). These results supported that CRAMP from neurons or exogenous $CRAMP_{1-39}$ had a protective effect against neuroinflammation. It did so by inhibiting the activation of microglia and astrocytes through the pro-resolving receptor FPR2, and subsequently dampening the encephalitogenic Th17 response.

Discussion

Our data reveal that CRAMP exerts opposite roles in neuroinflammation depending on its cellular source (Supplemental Figure 10). During EAE initiation, CRAMP is expressed locally by CNS-infiltrating neutrophils. Conditional knock-out mice unambiguously show that CRAMP from neutrophils is mandatory for the initiation of EAE. Our in vivo and in vitro experiments demonstrate that NET-associated CRAMP stimulates pro-Th17 response via cGAS/STING pathway. Recent studies support a role for neutrophils in MS (37). Circulating neutrophils in MS patients show a primed phenotype likely preceding their recruitment in the CNS where they may contribute to the local inflammation. In addition, MPO bound to DNA, which is considered a common marker of NETs, was found elevated in serum in MS patients (38, 39). In plasma, measures of neutrophil associated factors NE, CXCL1, and CXCL5 correlate with MS lesion burden and clinical disability (27). Molecular studies identified mRNA from the neutrophil-specific protein ASPRV1 in brain lesions, with higher amounts in severe MS compared to mild or moderate forms, and normal-appearing white matter (40). Neutrophils have been found in the cerebrospinal fluid (CSF) in MS patients during relapse, at an early disease stage, with correlation between the CSF neutrophils and IL-17A levels (41). Pediatric MS patients have neutrophils in the CSF (42), and interestingly in adults the neutrophils in the CSF tend to decrease with disease duration (41), both supporting a role for neutrophils locally in early disease. The detrimental role of neutrophils is also documented in two MS-related conditions: the neuromyelitis optica spectrum disorder (NMOSD) and the myelin oligodendrocyte glycoprotein antibody-associated disease (MOGAD). In both diseases, activation of neutrophils occurs in blood circulation, and the production of NETs into inflamed neural tissue is observed in brain from patients (43, 44). In rodent EAE, neutrophil numbers are expanded in the periphery, and in the CNS before and during the onset of symptoms (27). Depletion of neutrophils (45-47), inhibition of neutrophil migration by blocking of the

neutrophil chemokine receptor CXCR2 (48, 49), and depletion of neutrophil attracting cytokines such as IL-17 (50) and GM-CSF (51) significantly ameliorated the onset and severity of EAE.

The deleterious role of neutrophils in autoimmunity is mostly mediated by their production of NETs. Upon infection, neutrophils release chromatin material and granule content, including AMPs, to form net-like structures known as NETs (52). However, abnormal formation of NETs in sterile context contributes to many autoimmune diseases, including rheumatoid arthritis (RA), systemic lupus erythematosus (SLE), ANCA-associated vasculitis, Sjogren's syndrome (SjS), psoriasis, and type 1 diabetes (T1D) (28). Cathelicidin:nucleic acid complexes in NETs induce inflammatory cytokine production by myeloid immune cells promoting autoimmune responses (13-15). Human cathelicidin (LL-37) function as a cargo vehicle to transport extracellular nucleic acids into cells through membrane perturbation, permitting recognition by intracellular recognition systems within the endosome and cytosol such as TLR 3, 7, 8, 9, and cGAS-STING pathway (53, 54). cGAS has been identified as a sensor of NETs in myeloid immune cells, mediating their activation (15). Here, we show that NETs-associated CRAMP activates the cGAS/STING pathway in DCs stimulating the secretion of IL-6. It is noteworthy that in vitro, mouse CRAMP and human LL-37 cathelicidin showed ability to bind nucleic acids (55). Mouse CRAMP:nucleic acid complexes can stimulate plasmacytoid DC activation and type I IFN production in the context of skin injury (56), atherosclerosis (57), and autoimmune diabetes (14). Human LL-37:nucleic acid complexes can activate the cGAS-STING pathway in both human THP1 monocyte cells and murine RAW264.7 cells (58). This observation supports that the mechanism described in the mouse EAE model may be relevant to the human MS. It has been also demonstrated that cathelicidin from NETs enhances Th17 cell differentiation in dLNs through a direct effect on T cells, contributing to the development of EAE (31, 59). Together, these data support the contribution

of CRAMP from NETting neutrophils to EAE, both locally and in the periphery via the promotion of the Th17 response.

Our study also shows that CNS-resident cells, including neurons, express CRAMP, which dampens inflammatory cytokine expression by microglia and astrocytes to control disease severity. The immunoregulatory ability of cathelicidin has been largely documented in various contexts with several studies that have demonstrated that *Camp*$^{-/-}$ mice exhibit a more severe inflammatory phenotype compared to WT mice (60, 61). Cathelicidin and other AMPs modulate the immune response through multiple pathways including interference with TLR signaling, suppression of inflammatory cytokines, or induction of regulatory cytokines (62). In autoimmune context, cathelicidin from non-immune cells showed protective effect against RA and T1D through its ability to inhibit locally the expression of inflammatory cytokines by macrophages (63, 64). In the CNS, at steady state, *Camp*$^{-/-}$ mice showed an increased basal level of astrocyte activation, suggesting a role for brain-borne CRAMP in maintaining immune homeostasis (25). In infectious context, CNS bacterial infection or in vitro stimulation of glial cells by bacterial supernatants increased the expression of CRAMP by astrocytes, microglia, and meningeal cells (21, 24). CNS bacterial infection of *Camp*$^{-/-}$ mice led to a higher degree of glial cell activation accompanied by increased inflammatory cytokine expression in the CNS (25, 26). In the same infectious model, intracerebroventricular infusion of $CRAMP_{1-39}$ led to a decreased expression of inflammatory cytokines, while increasing the expression of the anti-inflammatory enzyme HO-1 in the CNS (65). In EAE, a parasitic cathelicidin-like peptide provided disease protection by reducing the expression of TNFα and IL-6 by macrophages (66). Two recent studies from the same group showed contradictory results regarding the role of cathelicidin in neuroinflammation. They showed that i.t. $CRAMP_{1-39}$ injection (30 µg at day 6 and day 9 post immunization) aggravated EAE and proposed that CRAMP stimulated IFNγ-primed microglia. It is worth noting that in this study multiple sources of CRAMP in the CNS

have also been identified, including neutrophils, astrocytes, neurons, and microglia. However, the relative function of CRAMP from these different cell sources was not deciphered (67). It is important to note that the dose of $CRAMP_{1-39}$ used in this study, was at least three times higher than the dose we used potentially causing direct tissue damage (68). In a subsequent study, the same group demonstrated that CRAMP was expressed by astrocytes, neurons, and microglia after in vivo LPS challenge. Intracerebroventricular $CRAMP_{1-39}$ treatment significantly inhibited LPS-mediated neuroinflammation, resulting in decreased expression of inflammatory cytokines. In vitro, consistent with our observations, $CRAMP_{1-39}$ treatment inhibited the expression of inflammatory cytokines by LPS-primed astrocytes and microglia (69).

Our in vitro experiments support that $CRAMP_{1-39}$ inhibits the activation of microglia and astrocytes through the FPR2 receptor. FPR2 is capable of recognizing a wide variety of ligands and has the ability to modulate both pro- and anti-inflammatory responses in the CNS, depending on the nature of these ligands (70). FPR2 expression has been described in different brain cell types, where its expression is significantly upregulated by pro-inflammatory stimuli (71). Activation of FPR2 with various agonists attenuates the effects of neuroinflammatory challenge by reducing the production of pro-inflammatory cytokines by microglia (72, 73). In line with our data, a recent study showed that treatment of primary murine microglia cells by FPR2 agonist prevented LPS-induced NFκB nuclear translocation, which decreased the expression of inflammatory cytokines (74). CRAMP is known to interact with FPR2 in several cell types (75), and our data suggest that CRAMP interaction with FPR2 suppresses inflammatory microglial activity. Taken together, our data and the literature support that the CRAMP:nucleic acid complex released by neutrophils promotes neuroinflammation via the cGAS-STING pathway, whereas the free form of CRAMP secreted by neurons controls neuroinflammation via the pro-resolving FPR2 expressed by microglia and astrocytes.

Finally, we show that butyrate, a microbiota-derived SCFAs, promotes CRAMP expression in neurons via FFAR2/3 receptors, decreased CRAMP expression in neutrophils, and accordingly has a protective role against EAE. Butyrate and other SCFAs are well-characterized cathelicidin inducer in various rodent and human cell types (76, 77). There is a significant body of evidence demonstrating that the gut microbiota plays a role in the development of MS and EAE with altered gut microbiota composition affecting immune function (1, 2, 78). Certain bacterial species contribute to the disease, while others have a dampening effect. Among protective species, butyrate-producing bacteria play a central role in promoting protective regulatory T (Treg) cells against EAE (79, 80). SCFAs, especially butyrate, promote intestinal Treg cells by inhibiting histone deacetylase (HDAC) activity at the *Foxp3* locus (81). Accordingly, butyrate has a protective effect against EAE with fewer Th17 cells in the CNS (82, 83). We propose, as demonstrated by us for T1D (64), that the protective effect of butyrate against EAE is also at least mediated by the stimulation of CRAMP expression by neurons. Butyrate can have EAE-protective effects through various mechanisms. For example, butyrate treatment in aged mice has been shown to promote neurogenesis in the hippocampus (84) and butyrate treatment in a rat model of middle cerebral artery occlusion has been shown to reduce neuronal apoptosis in the CNS *via* FFAR3 expressed by neurons (85). These results provide valuable insights and suggest potential avenues for future clinical trials targeting MS. Indeed, brain uptake of butyrate and other SCFAs has previously been demonstrated in rats following injection of ^{14}C-SCFAs into the carotid artery (86) and significant concentration of butyrate has been reported in the human brain at steady state (87). Brain concentrations of butyrate can be increased in mice after oral administration of live *Clostridium butyricum* (88), providing a potentially safe therapeutic strategy for MS. Butyrate is a FDA-approved drug and has demonstrated safety and efficacy in humans for treating

chronic bacterial infections (89), and several clinical trials are ongoing to test its efficacy against immune-mediated diseases.

Methods

Sex as a biological variable. Female mice were used in this study due to their heightened susceptibility to EAE. However, our findings are expected to be relevant to both sexes since male develop EAE with a similar physiopathology.

Mice and treatments. Female C57BL/6J, C57BL/6J CD45.1, *Camp*$^{-/-}$ C57BL/6J, Mrp8-Cre.*Camp*$^{f/f}$ and Mrp8-Cre.*Camp*^{WT} C57BL/6J between 10 to 14 weeks of ages were used, bred, and housed in specific opportunistic pathogen free conditions in Necker faculty animal facility. Mrp8-Cre mice were originally purchased from the Jackson laboratory (Strain #:021614) and crossed in our mouse facility, *Camp*$^{f/f}$ C57BL/6 mice were generated as follow: *Camp* gene consists of 4 exons on chromosome 9. *Camp*$^{tm1a(EUCOMM)HMGO}$ ES cells (JM8A3.N1; cell clone ID HEPD0722_1_E10; MGI:4950203) targeting the *Camp* locus were purchased from EUCOMM, injected into C57BL/6J embryos and transferred to recipient female mice. Male chimeric progeny was mated with C57BL/6J female mice to establish germ line transmission. Targeted mice (*Camp*$^{tm1a(EUCOMM)HMGO}$) were then crossed with B6;SJL-Tg(ACTFLPe)9205Dym/J (Strain #:003800) to generate mice with a 'flipped' *Camp* allele lacking the lacZ and neo vector cassettes. *Camp*$^{f/f}$ C57BL/6 mice were crossed with neutrophil-specific CRE recombinase line (B6.Cg-Tg(S100A8-cre,-EGFP)1Ilw/J (Mrp8-Cre^{Tg} mice, Strain #:021614). Breeding of Mrp8-Cre^{Tg}.*Camp*$^{wt/f}$ with *Camp*$^{f/f}$ generated mice with excision of *Camp* exons 2 – 4 in neutrophils (Mrp8-Cre^{Tg}.*Camp*$^{f/f}$ mice) and littermate controls (Mrp8-Cre^{neg}.*Camp*$^{f/f}$ mice). Recombinant mouse CRAMP$_{1–39}$ (ISRLAGLLRKGGEKIGEKLKKIGQKIKNFFQKLVPQPEQ) peptide and scrambled (sc)CRAMP$_{1–39}$ (KIGIEQLKGIKGIPEKRPGKRFKLVGEFSNQKALQKLQL) peptide were produced under aseptic conditions and provided after endotoxin removal processing (Innovagen). Peptides were administrated were administrated i.p. at the dose of 100 µg diluted

in 200 ml of PBS or i.t. at the dose of 10 µg diluted in 10 µl of PBS. Cl-amidine (5 $\mu g.g^{-1}$ body weight; Merck) or vehicle (PBS) were injected subcutaneously from day 7 to 17 post EAE induction. The 1A8 anti-Ly6G mAb was used to deplete neutrophils in EAE mice, whereas the 2A3 mAb served as the isotype control (BioXCell). Abs were administered i.p. 100 µg in 100 µL PBS every 3 days from 7 to 17 days post EAE immunization. Sodium butyrate (Sigma) was administrated in drinking water (10 $g.L^{-1}$) for 7 days.

EAE induction. EAE was induced by s.c. injections of 200 µg myelin oligodendrocyte glycoprotein $(MOG)_{35–55}$ (MEVGWYRSPFSRVVHLYRNGK; SB-peptide) in CFA (#AR002, Sigma Aldrich, containing 5 $mg.mL^{-1}$ heat-inactivated Mycobacterium tuberculosis H37Ra (# 231141, BD Biosciences)). An i.p. injection of 300 ng pertussis toxin (PTX; Gibco) was also administered on days 0 and 2 of the immunization. The severity of EAE was scored daily using a grading scale of 0–5: 0, unaffected; 0.5, partially limp tail; 1, paralyzed tail; 2, hindlimb paresis and loss in coordinated movement; 2.5, one hindlimb paralyzed; 3, both hindlimbs paralyzed; 3.5, hindlimbs paralyzed and weakness in forelimbs; 4, forelimbs paralyzed; 5, death or moribund mice requiring euthanasia. Mice with a grade 2 or above were provided with hydrated food on the floor of the cage.

Intrathecal administration of $CRAMP_{1-39}$ and adeno-associated virus Camp shRNA. Adeno-associated virus serotype 9 (AAV9)-GFP-U6-m*Camp*-shRNA and AAV9-GFP-U6-scrmb-shRNA ($4x10^{13}$ $GC.mL^{-1}$) were generated and validated by Vector Biosystems INC. Mice were injected i.t. with $CRAMP_{1–39}$ peptide (10 µg in 10 µL) or AAVs (10 µL) by a direct lumbar puncture within the intrathecal (i.t.) space of the spinal column performed with a 30-gauge needle connected to a 10-µL Hamilton syringe. The puncture of the dura was indicated by a reflexive flick of the tail.

Preparation of single-cell suspension. For spleens and lymph nodes, tissues were mashed through a 100-µM strainer, cells washed with HBSS 10% FBS and red blood cells were lysed using RBC Lysis Buffer (Biologend). Immune cells from the spinal cord were isolated using the multi-tissue dissociation kit 1 (Miltenyi Biotec), neural cells from the spinal cord or brain were isolated using the adult brain dissociation kit (Miltenyi Biotec); both combined with gentleMACS^{TM} Octo dissociator with heaters according to the manufacturer's instructions.

Flow cytometry. Single cell suspensions were prepared from various tissues, surface staining was performed after FcγRII/III blocking (anti-CD16/CD32, TruStain FcX™, Biolegend) for 5 min at 4°C and were surface stained for 30 min at 4°C. In all experiments dead cells were excluded using Fixable Viability Dye (eBioscience). Conjugated antibodies against the following antigens were used: CD45 (clone 30-F11, Biolegend), CD11c (NF18, Biolegend), CD11b (M1/70, Biolegend), Ly6G (IA8, Biolegend), F4/80 (BM8, Biolegend), CD19 (6D5, Biolgend), TCRβ (H57-597, Biolegend), CD4 (GK1.5, Biolegend), CD44 (IM7, Biolegend), CD86 (GL-1, Biolegend), CD62L (MEL-14, Biolegend, #104428, 1:300), NeuN (3A4C1, ThermoFisher), GFAP (2.2B10, eBioscience), Tmem119 (V3RT1Gosz, eBioscience). Unconjugated antibody for CRAMP (PA-CRPL-100, Innovagen) was used followed by donkey-anti-rabbit-IgG (poly4064, Biolegend) staining. $MOG_{35–55}$-specific CD4 T cells were stained using the T-Select I-A^b $MOG_{35–55}$ Tetramer-PE (MBL) according to the manufacturer instructions. For cytokine expression, cell suspensions were incubated 6 h at 37°C with cell stimulation cocktail (eBioscience) in the presence of a protein transport inhibitor cocktail (eBioscience), surface stained, fixed and then intracellularly stained with anti-IL-17A (R&D, 881309) and anti-IFNγ mAbs (eBioscience, XMG1.2) using the intracellular staining kit (Biolegend).

RT-qPCR. Total RNA was isolated using the Nucleospin RNA+ kit (#740984, Macherey-Nagel) from spinal cord. RNA was reverse transcribed to synthesized cDNA using the high-capacity cDNA reverse transcription kit (#4368814, ThermoFisher) and measurements were performed by qPCR using ONEGreen® fast qPCR premix (#OZYA008, Ozyme) on a Azure Cielo™ 6 Real-time PCR system. Resulting levels of fluorescence were submitted to relative quantification by normalization against a housekeeping gene (GAPDH) and expressed as $2^{-(\Delta CT)}$ values.

In vitro NET generation. Neutrophils were isolated from bone marrow using the Neutrophil Isolation Kit (#130-097-658, Miltenyi Biotec) as per the manufacturer's instructions. Neutrophils were plated at 2×10^6 cells/well in 12-well plates in 500 µL per well in RPMI 2% FBS. 3.8 µM A23187 ionophore (#C7522, Sigma) was added to plated neutrophils before incubation for 4 h at 37 °C, 5% CO2 to induce NET formation. Supernatants were carefully discarded, and the remaining NETs were gently washed twice with 1 mL PBS and detached from cells, by digestion with ALU1 (#R0137S, NEB) at 4 U/mL in 400 mL per well in RPMI for 20 min at 37 °C. Digested NETs were collected by mixing vigorously and subsequent centrifugation at 300×g for 5 min at 4 °C. Soluble NETs in cell-free supernatant were collected into fresh tubes and stored at −20 °C until use. A similar protocol was used to visualize NETs. Neutrophils were plated on round glass coverslips for 2h before staining with anti-CRAMP pAb (#PA-CRPL, Rabbit, Innovagen). After washing, slides were then incubated with donkey anti-rabbit Ab (#20966, Biotum). Nucleic acids were stained with SYTOX™ green (#S7020, Thermofischer).

Splenocyte culture and transfer. Single-cell suspension was prepared from spleen 10 days after EAE induction of C57BL/6 mice or in specific experiment of C57BL/6 CD45.1 mice. Cells were cultured for 3 days with 30 µg.mL^{-1} $MOG_{35–55}$ peptide (SB-peptide) in IMDM 10% FBS, 2 mM L-glutamine, 10 units/mL penicillin, 10 µg/mL streptomycin, 10 mM Hepes, 0.1% sodium pyruvate, 0.1% β-mercaptoethanol (all from Merck) containing 20 ng.mL^{-1} mouse IL-12, 20 ng.mL^{-1} mouse IL-23 (all from Biolegend) and 10 µg.mL^{-1} anti-mouse IFNγ mAb (#BE0055, BioXcell). In some cultures, increasing doses (0.1 to 30 µg.mL^{-1}) of $CRAMP_{1–39}$ (Innovagen) or NETs (50 µL per 200 µL) were added. For transfer experiments, 300x10^6 cells were cultured in 100 mL, washed, and 50x10^6 cells were injected i.p. in naïve mice to induce EAE. The average frequency of $CD4^+$ T cells in the culture was 10.9% at day 0 and 15.7% at day 3. For cytokine measurement, 2x10^5 cells were plated per well of round-bottom 96-well plate. Cytokines were quantitated in the cell culture supernatants with a Legendplex mouse inflammation panel assay (#740446, Biolegend) according to the manufacturer instructions.

Bone-marrow derived dendritic cell (BMDC) generation and stimulation. BMDCs were prepared from progenitor cells isolated from the femurs and tibias of 8-wk-old female mice. Briefly, BM cells were plated on six-well low-cluster plates in RPMI1640 medium containing 10% FCS and 1% penicillin/streptomycin and supplemented with 10 ng.mL^{-1} murine GM-CSF (R&D Systems) for 8 days. In some conditions, NETs (50 µL per 500 µL), cGAS inhibitor TDI-6570 (10 µM, Invivogen), or multi-specific TLR9, AIM2 and cGAS antagonist ODN A151 (10 µM, Invivogen) were added 18 h before analysis. Cytokines were quantitated in the cell culture supernatants with a Legendplex mouse inflammation panel assay (Biolegend) according to the manufacturer instructions.

OVA immunization and proliferation of OT-II T cells. $CD4^+$ OT-II T cells were isolated from C57BL/6-Tg(TcraTcrb)425Cbn/Crl mice using naive CD4 T Cell Isolation Kit (#130-104-454, Miltenyi Biotech) and labeled with CellTrace™ CFSE (#C34554, Thermo Fisher Scientific) according to the manufacturer instructions. OT-II cells were transferred i.v. 1 day prior to immunization with 100 µg ovalbumin (OVA) emulsified in CFA in rear footpads. Seven days later, single-cell suspension generated from the dLNs and OT-II cell division analyzed by flow cytometry.

Immunofluorescence staining. The spinal cord, and cervical lymph nodes were isolated and frozen in OCT (#4583, Sakura Finetek) in liquid nitrogen to be cryo-sectioned (5 µM). Frozen sections were air dried for 10 min before fixation in 4% PFA for additional 10 min. Slides were permeabilized with PBS 0.1% Triton X-100 (Sigma) and blocked with commercial blocking buffer (#ab64226, Abcam) for 1 hour at room temperature (RT), then primary antibodies were incubated in 10% donkey serum overnight at 4˚C. Primary antibodies used are: CRAMP (#PA-CRPL, Rabbit, Innovagen), anti-Ly6G (NIMP-R14, Rat, Abcam), MAP2 (AP-20, Mouse, Abcam), GFAP (#ab4674, Chicken, Abcam). After washing, slides were then incubated with a combination of the following secondary antibodies coupled with CF® dyes: donkey anti-rat (#20843), donkey anti-rabbit (#20966), donkey anti-chicken (#20166) and donkey anti-mouse (#20014) (all from Biotum). Nuclei were stained with DAPI (#D1306, Molecular probes). Image acquisition was performed on SFR Necker Imaging Facility using a Zeiss Spinning disk microscope.

Primary glial cell culture. For primary microglial cell cultures, the brains of 3-day-old mice were homogenized and mechanically disrupted with a nylon mesh and filtered through a 70 µM cell strainer. The obtained mixed glial cells were seeded in culture flasks and grown in an

incubator at 37°C with 5% CO2 in DMEM, 10% FBS, 200 mM L-glutamine, 100 $U.mL^{-1}$ penicillin, 0.1 $mg.mL^{-1}$ streptomycin, OPI supplement (oxalacetic acid, pyruvate, insulin; # O5003, Sigma). Culture media was changed initially at day 5 and then every 3 days. After 14 days of culture, primary microglia were obtained from mixed glial cells by shaking overnight at 200 rpm at 37°C and maintained in complete medium. Cells were activated with LPS for 24 h before addition of 10 $\mu g.mL^{-1}$ $CRAMP_{1–39}$ or vehicle for additional 24h. Astrocytes were isolated from adult brain using the Adult Brain Dissociation Kit (#130-107-667, Miltenyi Biotec) according to the manufacturer instructions. Isolated astrocytes, 10^5 cells, were maintained in culture in 24-well plate in MACS Neuro Medium containing 2% MACS Neuro Brew-21, 1% penicillin/streptomycin and 0.5 mM L-Glutamine. Cells were activated with LPS for 24h before addition of 10 $\mu g.mL^{-1}$ $CRAMP_{1–39}$ or vehicle for additional 24h. In some conditions, FPR2 antagonist WRW4 or P2X7R antagonist JNJ-47695567 (both from Tocris Bioscience) was added 2h before CRAMP addition. Cytokines were quantitated in the cell culture supernatants with a Legendplex mouse macrophage panel assay (#740846, Biolegend) according to the manufacturer instructions.

In vitro culture of NSC-34 neuron cell line. For neuron differentiation, NSC-34 cells (#CLU140-A, Tebubio) were seeded at a concentration of $5x10^4$ cells per cm^2 in collagen-coated plates. The proliferation medium (DMEM, 10% FBS, 100 $U.mL^{-1}$ penicillin, 0.1 $mg.mL^{-1}$ streptomycin) was replaced 24h after seeding by differentiation medium (DMEM/F-12 (ham), 1% FBS, 1% modified Eagle's medium non-essential amino acids, and 1 µM retinoic acid (RA, #554720, Sigma)). Cells were allowed to differentiate for 4 days. In some experiments, CRAMP expression was analyzed by confocal microscopy as described in the Immunofluorescence staining section. Primary antibodies used are: CRAMP (#PA-CRPL, Rabbit, Innovagen), MAP2 (#ab5392, Chicken, Abcam), Synaptophysin (SP11, Mouse,

ThermoFisher). After washing, slides were then incubated with a combination of the following secondary antibodies coupled with CF® dyes: donkey anti-rabbit (#20966), donkey anti-chicken (#20166) and donkey anti-mouse (#20046) (all from Biotum). Nuclei were stained with DAPI (#D1306, Molecular probes). In some experiments, the differentiation medium was replaced by RA-free medium and cells were stimulated for 24h by 10 $\mu g.mL^{-1}$ of each SCFAs: sodium butyrate, sodium acetate or sodium propionate. The GRP43 antagonist GLPG 0974 (1 µM, Tocris) was added to the culture 2h before the addition of the SCFAs. Then *Camp* mRNA expression was analyzed by RT-qPCR.

Statistical analysis. Comparison between each group was performed using the non-parametric Mann-Whitney U-test, or Kruskal-Wallis test followed up by Dunn's post-test when more than 2 groups were compared. For evaluating differences between EAE scores over time, a two-way ANOVA with Tukey's multiple comparisons test was used. P values < 0.05 were considered statistically significant. All data were analyzed using GraphPad Prism v9 software.

Study approval. All animal experimental protocols were approved by the French ethic committee for animal experimentation (APAFIS#19833-2018031214353174).

Data availability. For all data values for all graphs, see the Supporting Data Values file.

Authors contributions

SCV and EE performed, analyzed experiments, interpreted data and wrote the paper with general assistance of JD. FR, KM, CBT, and AP performed specific in vitro experiments. MT performed biodistribution experiments. DRG provided expertise in AAV-shRNA design and intrathecal injection. SF and FO provided intellectual input and expertise to analyze

experiments and wrote the paper. RL and JD designed the project, interpreted data, and wrote the paper. Authorship order among the two co–first authors was determined by who initiated the work.

Acknowledgments

The authors greatly acknowledge the SFR Necker facilities and the EUCOMM consortium for ES cells. This work was supported by funds from France Sclérose En Plaques Fondation (ARSEP 2016/2020).

Conflict-of-interest statement

“The authors have declared that no conflict of interest exists.”

References

1. Berer K, Mues M, Koutrolos M, Rasbi ZA, Boziki M, Johner C, Wekerle H, and Krishnamoorthy G. Commensal microbiota and myelin autoantigen cooperate to trigger autoimmune demyelination. *Nature.* 2011;479(7374):538-41.
2. i MCEasbue, and i MC. Gut microbiome of multiple sclerosis patients and paired household healthy controls reveal associations with disease risk and course. *Cell.* 2022;185(19):3467-86 e16.
3. Berger JR, and Markowitz C. Deciding on the Best Multiple Sclerosis Therapy: Tough Choices. *JAMA Neurol.* 2018.
4. Fan Y, and Zhang J. Dietary Modulation of Intestinal Microbiota: Future Opportunities in Experimental Autoimmune Encephalomyelitis and Multiple Sclerosis. *Frontiers in microbiology.* 2019;10(740.
5. Codarri L, Greter M, and Becher B. Communication between pathogenic T cells and myeloid cells in neuroinflammatory disease. *Trends Immunol.* 2013;34(3):114-9.
6. Ransohoff RM. Animal models of multiple sclerosis: the good, the bad and the bottom line. *Nat Neurosci.* 2012;15(8):1074-7.
7. Mrdjen D, Pavlovic A, Hartmann FJ, Schreiner B, Utz SG, Leung BP, Lelios I, Heppner FL, Kipnis J, Merkler D, et al. High-Dimensional Single-Cell Mapping of Central Nervous System Immune Cells Reveals Distinct Myeloid Subsets in Health, Aging, and Disease. *Immunity.* 2018;48(2):380-95 e6.
8. Hultmark D, Steiner H, Rasmuson T, and Boman HG. Insect immunity. Purification and properties of three inducible bactericidal proteins from hemolymph of immunized pupae of Hyalophora cecropia. *Eur J Biochem.* 1980;106(1):7-16.
9. Gallo RL, and Hooper LV. Epithelial antimicrobial defence of the skin and intestine. *Nat Rev Immunol.* 2012;12(7):503-16.

10. Liang WJ, Enee E, Andre-Vallee C, Falcone M, Sun J, and Diana J. Intestinal Cathelicidin Antimicrobial Peptide Shapes a Protective Neonatal Gut Microbiota Against Pancreatic Autoimmunity. *Gastroenterology.* 2022;162(4):1288-+.

11. Hancock RE, Haney EF, and Gill EE. The immunology of host defence peptides: beyond antimicrobial activity. *Nat Rev Immunol.* 2016;16(5):321-34.

12. Pinegin B, Vorobjeva N, and Pinegin V. Neutrophil extracellular traps and their role in the development of chronic inflammation and autoimmunity. *Autoimmun Rev.* 2015.

13. Lande R, Ganguly D, Facchinetti V, Frasca L, Conrad C, Gregorio J, Meller S, Chamilos G, Sebasigari R, Riccieri V, et al. Neutrophils activate plasmacytoid dendritic cells by releasing self-DNA-peptide complexes in systemic lupus erythematosus. *Sci Transl Med.* 2011;3(73):73ra19.

14. Diana J, Simoni Y, Furio L, Beaudoin L, Agerberth B, Barrat F, and Lehuen A. Crosstalk between neutrophils, B-1a cells and plasmacytoid dendritic cells initiates autoimmune diabetes. *Nat Med.* 2013;19(1):65-73.

15. Apel F, Andreeva L, Knackstedt LS, Streeck R, Frese CK, Goosmann C, Hopfner KP, and Zychlinsky A. The cytosolic DNA sensor cGAS recognizes neutrophil extracellular traps. *Sci Signal.* 2021;14(673).

16. Liang W, and Diana J. The Dual Role of Antimicrobial Peptides in Autoimmunity. *Frontiers in immunology.* 2020;11(2077.

17. Su Y, Zhang K, and Schluesener HJ. Antimicrobial peptides in the brain. *Arch Immunol Ther Exp (Warsz).* 2010;58(5):365-77.

18. Stuart BAR, Franitza AL, and E L. Regulatory Roles of Antimicrobial Peptides in the Nervous System: Implications for Neuronal Aging. *Front Cell Neurosci.* 2022;16(843790.

19. Bergman P, Termen S, Johansson L, Nystrom L, Arenas E, Jonsson AB, Hokfelt T, Gudmundsson GH, and Agerberth B. The antimicrobial peptide rCRAMP is present in the central nervous system of the rat. *J Neurochem.* 2005;93(5):1132-40.

20. Bergman P, Johansson L, Wan H, Jones A, Gallo RL, Gudmundsson GH, Hokfelt T, Jonsson AB, and Agerberth B. Induction of the antimicrobial peptide CRAMP in the blood-brain barrier and meninges after meningococcal infection. *Infect Immun.* 2006;74(12):6982-91.

21. Brandenburg LO, Varoga D, Nicolaeva N, Leib SL, Wilms H, Podschun R, Wruck CJ, Schroder JM, Pufe T, and Lucius R. Role of glial cells in the functional expression of LL-37/rat cathelin-related antimicrobial peptide in meningitis. *J Neuropathol Exp Neurol.* 2008;67(11):1041-54.

22. Williams WM, Castellani RJ, Weinberg A, Perry G, and Smith MA. Do beta-defensins and other antimicrobial peptides play a role in neuroimmune function and neurodegeneration? *ScientificWorldJournal.* 2012;2012(905785.

23. Appelgren D, Enocsson H, Skogman BH, Nordberg M, Perander L, Nyman D, Nyberg C, Knopf J, Munoz LE, Sjowall C, et al. Neutrophil Extracellular Traps (NETs) in the Cerebrospinal Fluid Samples from Children and Adults with Central Nervous System Infections. *Cells.* 2019;9(1).

24. Brandenburg LO, Varoga D, Nicolaeva N, Leib SL, Podschun R, Wruck CJ, Wilms H, Lucius R, and Pufe T. Expression and regulation of antimicrobial peptide rCRAMP after bacterial infection in primary rat meningeal cells. *J Neuroimmunol.* 2009;217(1-2):55-64.

25. Merres J, Hoss J, Albrecht LJ, Kress E, Soehnlein O, Jansen S, Pufe T, Tauber SC, and Brandenburg LO. Role of the cathelicidin-related antimicrobial peptide in inflammation

and mortality in a mouse model of bacterial meningitis. *J Innate Immun.* 2014;6(2):205-18.

26. Kress E, Merres J, Albrecht LJ, Hammerschmidt S, Pufe T, Tauber SC, and Brandenburg LO. CRAMP deficiency leads to a pro-inflammatory phenotype and impaired phagocytosis after exposure to bacterial meningitis pathogens. *Cell Commun Signal.* 2017;15(1):32.

27. Rumble JM, Huber AK, Krishnamoorthy G, Srinivasan A, Giles DA, Zhang X, Wang L, and Segal BM. Neutrophil-related factors as biomarkers in EAE and MS. *J Exp Med.* 2015;212(1):23-35.

28. Wigerblad G, and Kaplan MJ. Neutrophil extracellular traps in systemic autoimmune and autoinflammatory diseases. *Nat Rev Immunol.* 2023;23(5):274-88.

29. Shafqat A, Noor Eddin A, Adi G, Al-Rimawi M, Abdul Rab S, Abu-Shaar M, Adi K, Alkattan K, and Yaqinuddin A. Neutrophil extracellular traps in central nervous system pathologies: A mini review. *Front Med (Lausanne).* 2023;10(1083242.

30. Geeraerts T, Guilbeau-Frugier C, Garcia C, Memier V, Raposo N, Bonneville F, Gales C, Darcourt J, Voisin S, Ribes A, et al. Immunohistologic Features of Cerebral Venous Thrombosis Due to Vaccine-Induced Immune Thrombotic Thrombocytopenia. *Neurol Neuroimmunol Neuroinflamm.* 2023;10(4).

31. Minns D, Smith KJ, Alessandrini V, Hardisty G, Melrose L, Jackson-Jones L, MacDonald AS, Davidson DJ, and Gwyer Findlay E. The neutrophil antimicrobial peptide cathelicidin promotes Th17 differentiation. *Nature communications.* 2021;12(1):1285.

32. Alford MA, Baquir B, Santana FL, Haney EF, and Hancock REW. Cathelicidin Host Defense Peptides and Inflammatory Signaling: Striking a Balance. *Frontiers in microbiology.* 2020;11(1902.

33. Kida Y, Shimizu T, and Kuwano K. Sodium butyrate up-regulates cathelicidin gene expression via activator protein-1 and histone acetylation at the promoter region in a human lung epithelial cell line, EBC-1. *Mol Immunol.* 2006;43(12):1972-81.

34. Jahan-Abad AJ, Karima S, Shateri S, Baram SM, Rajaei S, Morteza-Zadeh P, Borhani-Haghighi M, Salari AA, Nikzamir A, and Gorji A. Serum pro-inflammatory and anti-inflammatory cytokines and the pathogenesis of experimental autoimmune encephalomyelitis. *Neuropathology.* 2020;40(1):84-92.

35. Ji Z, Wu S, Xu Y, Qi J, Su X, and Shen L. Obesity Promotes EAE Through IL-6 and CCL-2-Mediated T Cells Infiltration. *Frontiers in immunology.* 2019;10(1881.

36. Scheenstra MR, van Harten RM, Veldhuizen EJA, Haagsman HP, and Coorens M. Cathelicidins Modulate TLR-Activation and Inflammation. *Frontiers in immunology.* 2020;11(1137.

37. Woodberry T, Bouffler SE, Wilson AS, Buckland RL, and Brustle A. The Emerging Role of Neutrophil Granulocytes in Multiple Sclerosis. *J Clin Med.* 2018;7(12).

38. Naegele M, Tillack K, Reinhardt S, Schippling S, Martin R, and Sospedra M. Neutrophils in multiple sclerosis are characterized by a primed phenotype. *J Neuroimmunol.* 2012;242(1-2):60-71.

39. Minohara M, Matsuoka T, Li W, Osoegawa M, Ishizu T, Ohyagi Y, and Kira J. Upregulation of myeloperoxidase in patients with opticospinal multiple sclerosis: positive correlation with disease severity. *J Neuroimmunol.* 2006;178(1-2):156-60.

40. Whittaker Hawkins RF, Patenaude A, Dumas A, Jain R, Tesfagiorgis Y, Kerfoot S, Matsui T, Gunzer M, Poubelle PE, Larochelle C, et al. ICAM1+ neutrophils promote chronic inflammation via ASPRV1 in B cell-dependent autoimmune encephalomyelitis. *JCI Insight.* 2017;2(23).

41. Kostic M, Dzopalic T, Zivanovic S, Zivkovic N, Cvetanovic A, Stojanovic I, Vojinovic S, Marjanovic G, Savic V, and Colic M. IL-17 and glutamate excitotoxicity in the pathogenesis of multiple sclerosis. *Scand J Immunol.* 2014;79(3):181-6.

42. Chabas D, Ness J, Belman A, Yeh EA, Kuntz N, Gorman MP, Strober JB, De Kouchkovsky I, McCulloch C, Chitnis T, et al. Younger children with MS have a distinct CSF inflammatory profile at disease onset. *Neurology.* 2010;74(5):399-405.

43. Murata H, Kinoshita M, Yasumizu Y, Motooka D, Beppu S, Shiraishi N, Sugiyama Y, Kihara K, Tada S, Koda T, et al. Cell-Free DNA Derived From Neutrophils Triggers Type 1 Interferon Signature in Neuromyelitis Optica Spectrum Disorder. *Neurol Neuroimmunol Neuroinflamm.* 2022;9(3).

44. Hoftberger R, Guo Y, Flanagan EP, Lopez-Chiriboga AS, Endmayr V, Hochmeister S, Joldic D, Pittock SJ, Tillema JM, Gorman M, et al. The pathology of central nervous system inflammatory demyelinating disease accompanying myelin oligodendrocyte glycoprotein autoantibody. *Acta Neuropathol.* 2020;139(5):875-92.

45. Aube B, Levesque SA, Pare A, Chamma E, Kebir H, Gorina R, Lecuyer MA, Alvarez JI, De Koninck Y, Engelhardt B, et al. Neutrophils mediate blood-spinal cord barrier disruption in demyelinating neuroinflammatory diseases. *J Immunol.* 2014;193(5):2438-54.

46. McColl SR, Staykova MA, Wozniak A, Fordham S, Bruce J, and Willenborg DO. Treatment with anti-granulocyte antibodies inhibits the effector phase of experimental autoimmune encephalomyelitis. *J Immunol.* 1998;161(11):6421-6.

47. Shen P, Rother M, Stervbo U, Lampropoulou V, Calderon-Gomez E, Roch T, Hilgenberg E, Ries S, Kuhl AA, Jouneau L, et al. Toll-like receptors control the accumulation of neutrophils in lymph nodes that expand CD4(+) T cells during experimental autoimmune encephalomyelitis. *Eur J Immunol.* 2023;53(2):e2250059.

48. Carlson T, Kroenke M, Rao P, Lane TE, and Segal B. The Th17-ELR+ CXC chemokine pathway is essential for the development of central nervous system autoimmune disease. *J Exp Med.* 2008;205(4):811-23.

49. Liu Y, Holdbrooks AT, Meares GP, Buckley JA, Benveniste EN, and Qin H. Preferential Recruitment of Neutrophils into the Cerebellum and Brainstem Contributes to the Atypical Experimental Autoimmune Encephalomyelitis Phenotype. *J Immunol.* 2015;195(3):841-52.

50. Komiyama Y, Nakae S, Matsuki T, Nambu A, Ishigame H, Kakuta S, Sudo K, and Iwakura Y. IL-17 plays an important role in the development of experimental autoimmune encephalomyelitis. *J Immunol.* 2006;177(1):566-73.

51. McQualter JL, Darwiche R, Ewing C, Onuki M, Kay TW, Hamilton JA, Reid HH, and Bernard CC. Granulocyte macrophage colony-stimulating factor: a new putative therapeutic target in multiple sclerosis. *J Exp Med.* 2001;194(7):873-82.

52. Brinkmann V, Reichard U, Goosmann C, Fauler B, Uhlemann Y, Weiss DS, Weinrauch Y, and Zychlinsky A. Neutrophil extracellular traps kill bacteria. *Science.* 2004;303(5663):1532-5.

53. Zielke C, Nielsen JE, Lin JS, and Barron AE. Between good and evil: Complexation of the human cathelicidin LL-37 with nucleic acids. *Biophys J.* 2024;123(11):1316-28.

54. Takahashi T, Kulkarni NN, Lee EY, Zhang LJ, Wong GCL, and Gallo RL. Cathelicidin promotes inflammation by enabling binding of self-RNA to cell surface scavenger receptors. *Scientific reports.* 2018;8(1):4032.

55. Wong A, Bryzek D, Dobosz E, Scavenius C, Svoboda P, Rapala-Kozik M, Lesner A, Frydrych I, Enghild J, Mydel P, et al. A Novel Biological Role for Peptidyl-Arginine Deiminases: Citrullination of Cathelicidin LL-37 Controls the Immunostimulatory Potential of Cell-Free DNA. *J Immunol.* 2018;200(7):2327-40.

56. Gregorio J, Meller S, Conrad C, Di Nardo A, Homey B, Lauerma A, Arai N, Gallo RL, Digiovanni J, and Gilliet M. Plasmacytoid dendritic cells sense skin injury and promote wound healing through type I interferons. *J Exp Med.* 2010;207(13):2921-30.

57. Doring Y, Manthey HD, Drechsler M, Lievens D, Megens RT, Soehnlein O, Busch M, Manca M, Koenen RR, Pelisek J, et al. Auto-antigenic protein-DNA complexes stimulate plasmacytoid dendritic cells to promote atherosclerosis. *Circulation.* 2012;125(13):1673-83.

58. Wei X, Zhang L, Yang Y, Hou Y, Xu Y, Wang Z, Su H, Han F, Han J, Liu P, et al. LL-37 transports immunoreactive cGAMP to activate STING signaling and enhance interferon-mediated host antiviral immunity. *Cell Rep.* 2022;39(9):110880.

59. Smith KJ, Minns D, McHugh BJ, Holloway RK, O'Connor R, Williams A, Melrose L, McPherson R, Miron VE, Davidson DJ, et al. The antimicrobial peptide cathelicidin drives development of experimental autoimmune encephalomyelitis in mice by affecting Th17 differentiation. *PLoS Biol.* 2022;20(8):e3001554.

60. Deng YY, Shamoon M, He Y, Bhatia M, and Sun J. Cathelicidin-related antimicrobial peptide modulates the severity of acute pancreatitis in mice. *Mol Med Rep.* 2016;13(5):3881-5.

61. Severino P, Ariga SK, Barbeiro HV, de Lima TM, de Paula Silva E, Barbeiro DF, Machado MCC, Nizet V, and Pinheiro da Silva F. Cathelicidin-deficient mice exhibit increased survival and upregulation of key inflammatory response genes following cecal ligation and puncture. *J Mol Med (Berl).* 2017;95(9):995-1003.

62. Mookherjee N, Anderson MA, Haagsman HP, and Davidson DJ. Antimicrobial host defence peptides: functions and clinical potential. *Nat Rev Drug Discov.* 2020;19(5):311-32.

63. Chow LN, Choi KY, Piyadasa H, Bossert M, Uzonna J, Klonisch T, and Mookherjee N. Human cathelicidin LL-37-derived peptide IG-19 confers protection in a murine model of collagen-induced arthritis. *Mol Immunol.* 2014;57(2):86-92.

64. Sun J, Furio L, Mecheri R, van der Does AM, Lundeberg E, Saveanu L, Chen Y, van Endert P, Agerberth B, and Diana J. Pancreatic beta-Cells Limit Autoimmune Diabetes via an Immunoregulatory Antimicrobial Peptide Expressed under the Influence of the Gut Microbiota. *Immunity.* 2015;43(2):304-17.

65. Dorr A, Kress E, Podschun R, Pufe T, Tauber SC, and Brandenburg LO. Intrathecal application of the antimicrobial peptide CRAMP reduced mortality and neuroinflammation in an experimental model of pneumococcal meningitis. *J Infect.* 2015;71(2):188-99.

66. Lund ME, Greer J, Dixit A, Alvarado R, McCauley-Winter P, To J, Tanaka A, Hutchinson AT, Robinson MW, Simpson AM, et al. A parasite-derived 68-mer peptide ameliorates autoimmune disease in murine models of Type 1 diabetes and multiple sclerosis. *Scientific reports.* 2016;6(37789.

67. Bhusal A, Nam Y, Seo D, Rahman MH, Hwang EM, Kim SC, Lee WH, and Suk K. Cathelicidin-related antimicrobial peptide promotes neuroinflammation through astrocyte-microglia communication in experimental autoimmune encephalomyelitis. *Glia.* 2022;70(10):1902-26.

68. Pinheiro da Silva F, Gallo RL, and Nizet V. Differing effects of exogenous or endogenous cathelicidin on macrophage toll-like receptor signaling. *Immunol Cell Biol.* 2009;87(6):496-500.

69. Bhusal A, Nam Y, Seo D, Lee WH, and Suk K. Cathelicidin-Related Antimicrobial Peptide Negatively Regulates Bacterial Endotoxin-Induced Glial Activation. *Cells.* 2022;11(23).

70. Tylek K, Trojan E, Regulska M, Lacivita E, Leopoldo M, and Basta-Kaim A. Formyl peptide receptor 2, as an important target for ligands triggering the inflammatory response regulation: a link to brain pathology. *Pharmacol Rep.* 2021;73(4):1004-19.

71. Pourbadie HG, Sayyah M, Khoshkholgh-Sima B, Choopani S, Nategh M, Motamedi F, and Shokrgozar MA. Early minor stimulation of microglial TLR2 and TLR4 receptors attenuates Alzheimer's disease-related cognitive deficit in rats: behavioral, molecular, and electrophysiological evidence. *Neurobiol Aging.* 2018;70(203-16.

72. Slowik A, Merres J, Elfgen A, Jansen S, Mohr F, Wruck CJ, Pufe T, and Brandenburg LO. Involvement of formyl peptide receptors in receptor for advanced glycation end products (RAGE)--and amyloid beta 1-42-induced signal transduction in glial cells. *Mol Neurodegener.* 2012;7(55.

73. Tylek K, Trojan E, Leskiewicz M, Regulska M, Bryniarska N, Curzytek K, Lacivita E, Leopoldo M, and Basta-Kaim A. Time-Dependent Protective and Pro-Resolving Effects of FPR2 Agonists on Lipopolysaccharide-Exposed Microglia Cells Involve Inhibition of NF-kappaB and MAPKs Pathways. *Cells.* 2021;10(9).

74. Wickstead ES, Elliott BT, Pokorny S, Biggs C, Getting SJ, and McArthur S. Stimulation of the Pro-Resolving Receptor Fpr2 Reverses Inflammatory Microglial Activity by Suppressing NFkappaB Activity. *Int J Mol Sci.* 2023;24(21).

75. Jeong YS, and Bae YS. Formyl peptide receptors in the mucosal immune system. *Exp Mol Med.* 2020;52(10):1694-704.

76. Schauber J, Svanholm C, Termen S, Iffland K, Menzel T, Scheppach W, Melcher R, Agerberth B, Luhrs H, and Gudmundsson GH. Expression of the cathelicidin LL-37 is modulated by short chain fatty acids in colonocytes: relevance of signalling pathways. *Gut.* 2003;52(5):735-41.

77. Steinmann J, Halldorsson S, Agerberth B, and Gudmundsson GH. Phenylbutyrate induces antimicrobial peptide expression. *Antimicrob Agents Chemother.* 2009;53(12):5127-33.

78. Correale J, Hohlfeld R, and Baranzini SE. The role of the gut microbiota in multiple sclerosis. *Nat Rev Neurol.* 2022;18(9):544-58.

79. Haghikia A, Jorg S, Duscha A, Berg J, Manzel A, Waschbisch A, Hammer A, Lee DH, May C, Wilck N, et al. Dietary Fatty Acids Directly Impact Central Nervous System Autoimmunity via the Small Intestine. *Immunity.* 2015;43(4):817-29.

80. Bianchimano P, Britton GJ, Wallach DS, Smith EM, Cox LM, Liu S, Iwanowski K, Weiner HL, Faith JJ, Clemente JC, et al. Mining the microbiota to identify gut commensals modulating neuroinflammation in a mouse model of multiple sclerosis. *Microbiome.* 2022;10(1):174.

81. Arpaia N, Campbell C, Fan X, Dikiy S, van der Veeken J, deRoos P, Liu H, Cross JR, Pfeffer K, Coffer PJ, et al. Metabolites produced by commensal bacteria promote peripheral regulatory T-cell generation. *Nature.* 2013;504(7480):451-5.

82. Mizuno M, Noto D, Kaga N, Chiba A, and Miyake S. The dual role of short fatty acid chains in the pathogenesis of autoimmune disease models. *PLoS One.* 2017;12(2):e0173032.

83. Wang C, Yang J, Xie L, Saimaier K, Zhuang W, Han M, Liu G, Lv J, Shi G, Li N, et al. Methyl Butyrate Alleviates Experimental Autoimmune Encephalomyelitis and Regulates the Balance of Effector T Cells and Regulatory T Cells. *Inflammation.* 2022;45(3):977-91.

84. Kundu P, Lee HU, Garcia-Perez I, Tay EXY, Kim H, Faylon LE, Martin KA, Purbojati R, Drautz-Moses DI, Ghosh S, et al. Neurogenesis and prolongevity signaling in young

germ-free mice transplanted with the gut microbiota of old mice. *Sci Transl Med.* 2019;11(518).

85. Zhou Z, Xu N, Matei N, McBride DW, Ding Y, Liang H, Tang J, and Zhang JH. Sodium butyrate attenuated neuronal apoptosis via GPR41/Gbetagamma/PI3K/Akt pathway after MCAO in rats. *J Cereb Blood Flow Metab.* 2021;41(2):267-81.

86. Oldendorf WH. Carrier-mediated blood-brain barrier transport of short-chain monocarboxylic organic acids. *Am J Physiol.* 1973;224(6):1450-3.

87. Bachmann C, Colombo JP, and Beruter J. Short chain fatty acids in plasma and brain: quantitative determination by gas chromatography. *Clin Chim Acta.* 1979;92(2):153-9.

88. Liu J, Sun J, Wang F, Yu X, Ling Z, Li H, Zhang H, Jin J, Chen W, Pang M, et al. Neuroprotective Effects of Clostridium butyricum against Vascular Dementia in Mice via Metabolic Butyrate. *BioMed research international.* 2015;2015(412946.

89. Chen J, and Vitetta L. The Role of Butyrate in Attenuating Pathobiont-Induced Hyperinflammation. *Immune network.* 2020;20(2):e15.

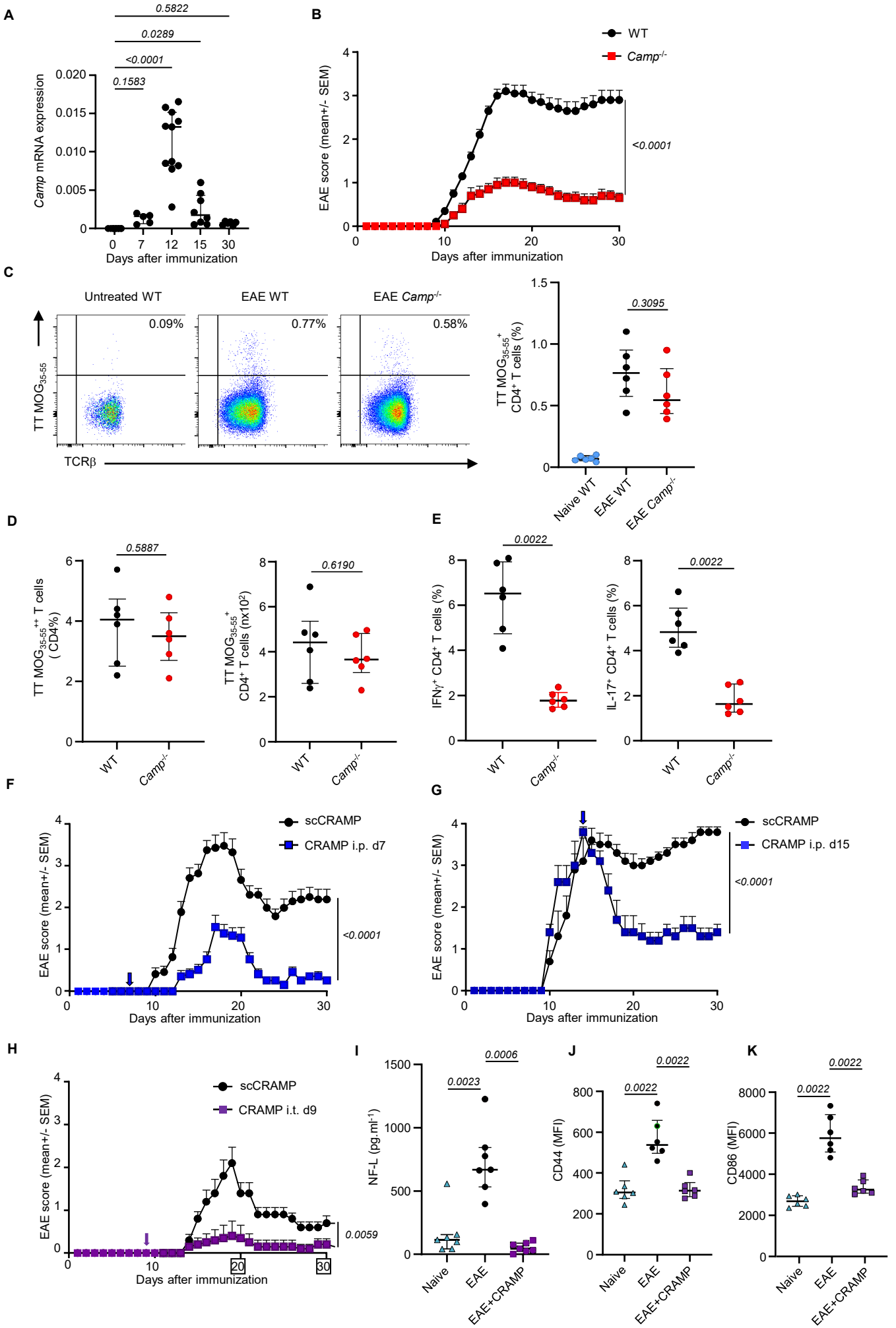
A
0.5822
0.0289
<0.0001
0.1583
Camp mRNA expression
0.020
0.015
0.010
0.005
0
0 7 12 15 30
Days after immunization
B
WT
Camp-/-
EAE score (mean+/- SEM)
<0.0001
Days after immunization
C
Untreated WT
EAE WT
EAE Camp-/-
0.09%
0.77%
0.58%
TT MOG35-55
TCRβ
TT MOG35-55+ CD4+ T cells (%)
0.3095
Naive WT
EAE WT
EAE Camp-/-
D
0.5887
TT MOG35-55++ T cells (CD4%)
0.6190
TT MOG35-55+ CD4+ T cells (nx10²)
WT
Camp-/-
E
0.0022
IFNγ+ CD4+ T cells (%)
0.0022
IL-17+ CD4+ T cells (%)
WT
Camp-/-
F
scCRAMP
CRAMP i.p. d7
EAE score (mean+/- SEM)
<0.0001
Days after immunization
G
scCRAMP
CRAMP i.p. d15
EAE score (mean+/- SEM)
<0.0001
Days after immunization
H
scCRAMP
CRAMP i.t. d9
EAE score (mean+/- SEM)
0.0059
Days after immunization
I
0.0006
0.0023
NF-L (pg.ml-1)
Naive
EAE
EAE+CRAMP
J
0.0022
0.0022
CD44 (MFI)
Naive
EAE
EAE+CRAMP
K
0.0022
0.0022
CD86 (MFI)
Naive
EAE
EAE+CRAMP

Figure 1 Opposite role of CRAMP during EAE. (A) mRNA expression of CRAMP was analyzed by RT-qPCR in spinal cord from C57BL/6 WT mice at different days after EAE induction. Data are the median +/− interquartile range of 5 to 11 independent mice per group from 4 independent experiments. (B) Camp-/- C57BL/6 mice and WT littermate controls (n=30 mice per group from 6 independent experiments) were immunized with MOG35-55 to induce EAE. Clinical scores are shown (mean ± SEM). (C−D) Cells from draining lymph nodes (C) or SC (D) were recovered on day 7 or 12 respectively, after EAE induction in Camp-/- and WT C57BL/6 mice and stained with I-Ab MOG35-55 tetramer. Data are the frequency and number of tetramer+ cells among CD45+ βTCR+ CD4+ cells. Median +/− interquartile range of 6 independent mice per group from 3 independent experiments is shown. (E) Frequency of IFN-γ+ and IL-17+ cells in CD4+ T cells recovered from the SC at day 12 after EAE induction in Camp-/- and WT C57BL/6 mice and restimulated for 6 hours with PMA/ionomycin. Median +/− interquartile range of 6 independent mice per group is shown from 3 independent experiments. (F−H) WT mice (n=15 mice per group from 3 independent experiments) were immunized with MOG35-55 to induce EAE. Mice were treated with CRAMP or scCRAMP i.p. at day 7 (F) or at day 15 (G) or i.t. at day 9 (H) after EAE induction. Clinical scores are shown (mean ± SEM). (I) Neurofilament light (NF-L) protein level was measured in the serum 15 days after EAE induction in WT mice treated as in (G) and in unmanipulated (naive) WT mice. Data are the median +/− interquartile range of 7 independent mice per group from 3 independent experiments. (J−K) Expression of CD44 on astrocytes (J) and CD86 on microglia (K) was determined by flow cytometry at day 15 post EAE induction in the SC of WT mice treated as in (G) and in unmanipulated (naive) WT mice. Data are the median +/− interquartile range of 6 independent mice per group from 3 independent experiments. Comparison between each group was performed using the non-parametric Mann-Whitney U-test, or Kruskal-Wallis test followed up by Dunn's post-test when more than 2 groups were compared. For evaluating differences between EAE scores over time, a two-way ANOVA with Tukey's multiple comparisons test was used.

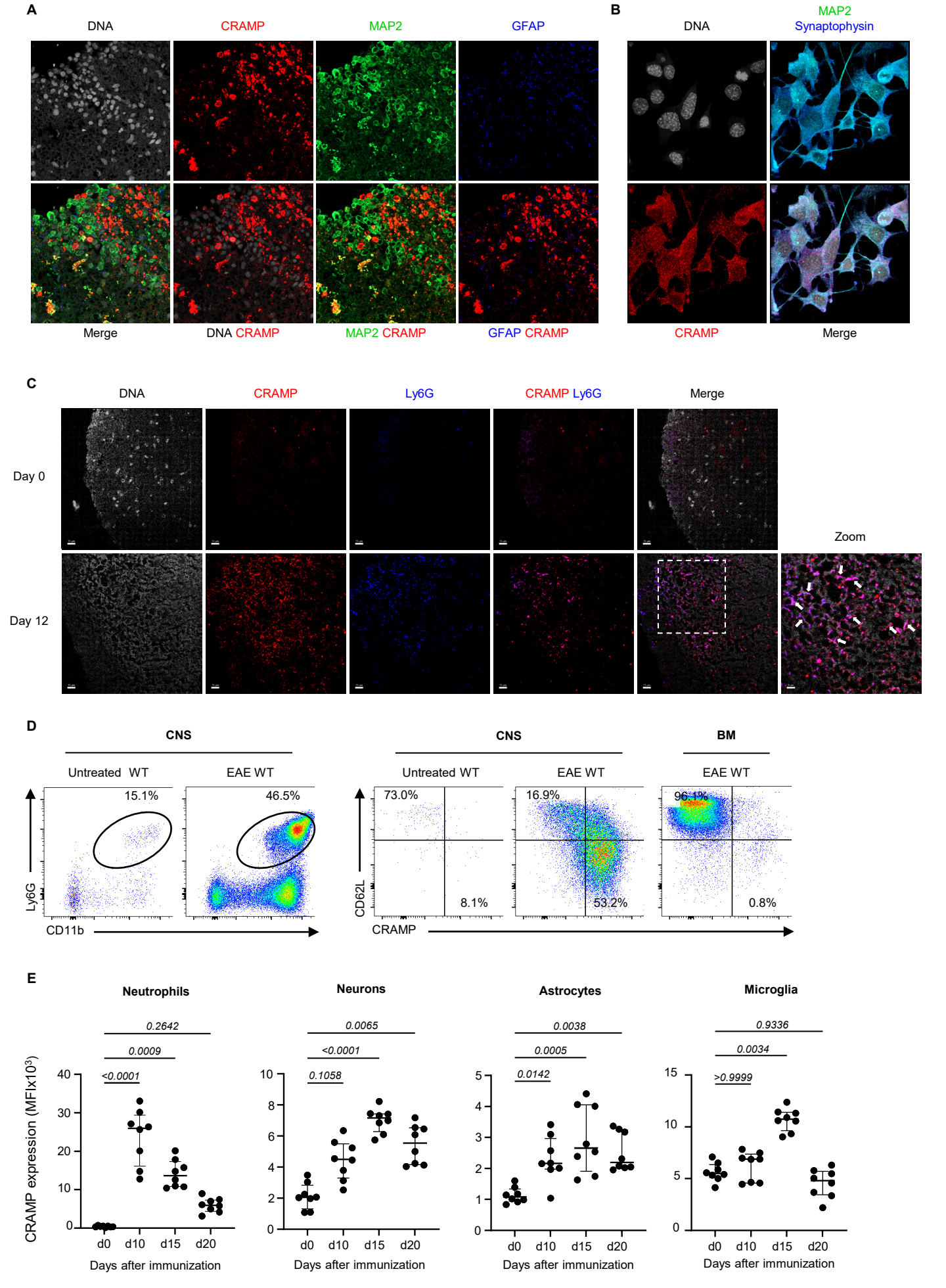
A
DNA
CRAMP
MAP2
GFAP
Merge
DNA CRAMP
MAP2 CRAMP
GFAP CRAMP
B
DNA
MAP2
Synaptophysin
CRAMP
Merge
C
DNA
CRAMP
Ly6G
CRAMP Ly6G
Merge
Zoom
Day 0
Day 12
D
CNS
Untreated WT
EAE WT
15.1%
46.5%
Ly6G
CD11b
CNS
BM
Untreated WT
EAE WT
EAE WT
73.0%
16.9%
96.1%
8.1%
53.2%
0.8%
CD62L
CRAMP
E
Neutrophils
Neurons
Astrocytes
Microglia
CRAMP expression (MFIx10³)
0.2642
0.0009
<0.0001
0.0065
<0.0001
0.1058
0.0038
0.0005
0.0142
0.9336
0.0034
>0.9999
d0
d10
d15
d20
Days after immunization

Figure 2 CRAMP is expressed in different cell types within the CNS during EAE. (A, C) Confocal microscopy images of SC section from WT mice immunized with MOG35-55 12 days earlier. Sections were stained for CRAMP (red), MAP2 (green), GFAP (blue) and DNA (grey) in (A) or for CRAMP (red), Ly6G (blue), and DNA (grey) in (C). Arrows indicate neutrophil extracellular traps. Data are representative of 3 independent experiments. Original magnification, x40. (B) Confocal microscopy images of motor neuron-like NSC-34 cells stained for CRAMP (red), MAP2 (green), Synaptophysin (blue) and DNA (grey) Data are representative of 3 independent experiments. Original magnification, x63. (D−E) Flow cytometry analysis of SC after EAE induction in WT mice. In D, 12 days after EAE induction, frequency of neutrophils (CD45+ CD11b+ Ly6G+ Ly6Clow) is shown in the left panel and the expression of CRAMP and CD62L by neutrophils is shown in the right panel. Bone marrow (BM) from tibia rich in immature neutrophils is shown as control. In E, the MFI of surface CRAMP expression on neutrophils, neurons (CD45− NeuN+), astrocytes (CD45− GFAP+), and microglia (CD45+ CD11b+ Tmem119+) is shown at different days post EAE induction. Data are the median +/− interquartile range of 8 independent mice per group from 3 independent experiments. Comparison between each group was performed using the non-parametric Mann-Whitney U-test, or Kruskal-Wallis test followed up by Dunn's post-test when more than 2 groups were compared.

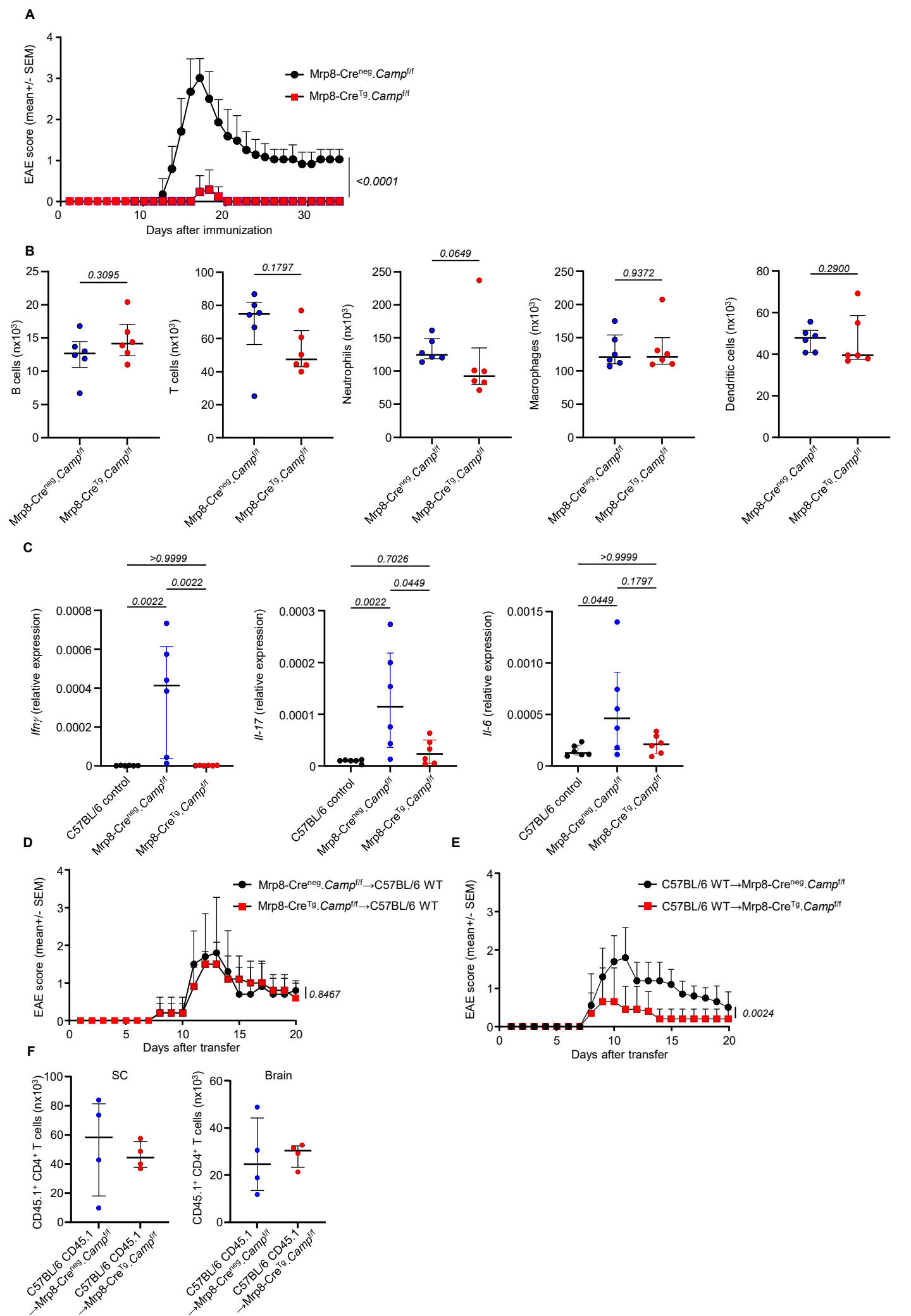
A
EAE score (mean+/- SEM)
Days after immunization
Mrp8-Cre^neg.Camp^f/f
Mrp8-Cre^Tg.Camp^f/f
<0.0001
B
B cells (nx10^3)
T cells (nx10^3)
Neutrophils (nx10^3)
Macrophages (nx10^3)
Dendritic cells (nx10^3)
0.3095
0.1797
0.0649
0.9372
0.2900
C
Ifnγ (relative expression)
Il-17 (relative expression)
Il-6 (relative expression)
>0.9999
0.0022
0.0022
0.7026
0.0449
0.0022
>0.9999
0.1797
0.0449
C57BL/6 control
D
EAE score (mean+/- SEM)
Days after transfer
Mrp8-Cre^neg.Camp^f/f→C57BL/6 WT
Mrp8-Cre^Tg.Camp^f/f→C57BL/6 WT
0.8467
E
EAE score (mean+/- SEM)
Days after transfer
C57BL/6 WT→Mrp8-Cre^neg.Camp^f/f
C57BL/6 WT→Mrp8-Cre^Tg.Camp^f/f
0.0024
F
SC
Brain
CD45.1+ CD4+ T cells (nx10^3)
C57BL/6 CD45.1 →Mrp8-Cre^neg.Camp^f/f
C57BL/6 CD45.1 →Mrp8-Cre^Tg.Camp^f/f

Figure 3 CRAMP from neutrophils is essential for EAE. (A) Mrp8-Creneg.Campf/f and Mrp8-CreTg.Campf/f mice (n=30 mice per group; 6 independent experiments) were immunized with MOG35-55 to induce EAE. Clinical scores are shown (mean ± SEM). (B) Flow cytometry analysis of SC 15 days after EAE induction. The absolute number of immune cells (CD45+), B cells (CD45+ CD19+), T cells (CD45+ □TCR+), neutrophils (CD45+ CD11b+ Ly6G+ Ly6Clow), macrophages (CD45+ CD11b+ Ly6G− F4/80+), and dendritic cells (CD45+ Ly6G− F4/80− CD11c+) is shown. Data are the median +/− interquartile range of 6 independent mice per group from 3 independent experiments. (C) mRNA expression of cytokines was analyzed by RT-qPCR in SC from Mrp8-Creneg.Campf/f and Mrp8-CreTg.Campf/f mice 15 days after EAE induction. Data are the median +/− interquartile range of 6 independent mice per group from 3 independent experiments. (D−F) Splenocytes were recovered 10 days after EAE induction in Mrp8-Creneg.Campf/f and Mrp8-CreTg.Campf/f mice (D) or C57BL/6 WT mice (E) or C57BL/6 CD45.1 mice (F). Cells were cultured for 3 days with MOG35-55 in pro-Th17 conditions and transferred in C57BL/6 WT mice (D) or in Mrp8-Creneg.Campf/f or Mrp8-CreTg.Campf/f mice (E−F). Clinical scores are shown (mean ± SEM) (n=15 mice per group from 3 independent experiments) in D, E. Number of CD45.1+ CD4+ T cells in the SC and the brain 7 days after transfer is shown in F. Comparison between each group was performed using the non-parametric Mann-Whitney U-test, or Kruskal-Wallis test followed up by Dunn's post-test when more than 2 groups were compared. For evaluating differences between EAE scores over time, a two-way ANOVA with Tukey's multiple comparisons test was used.

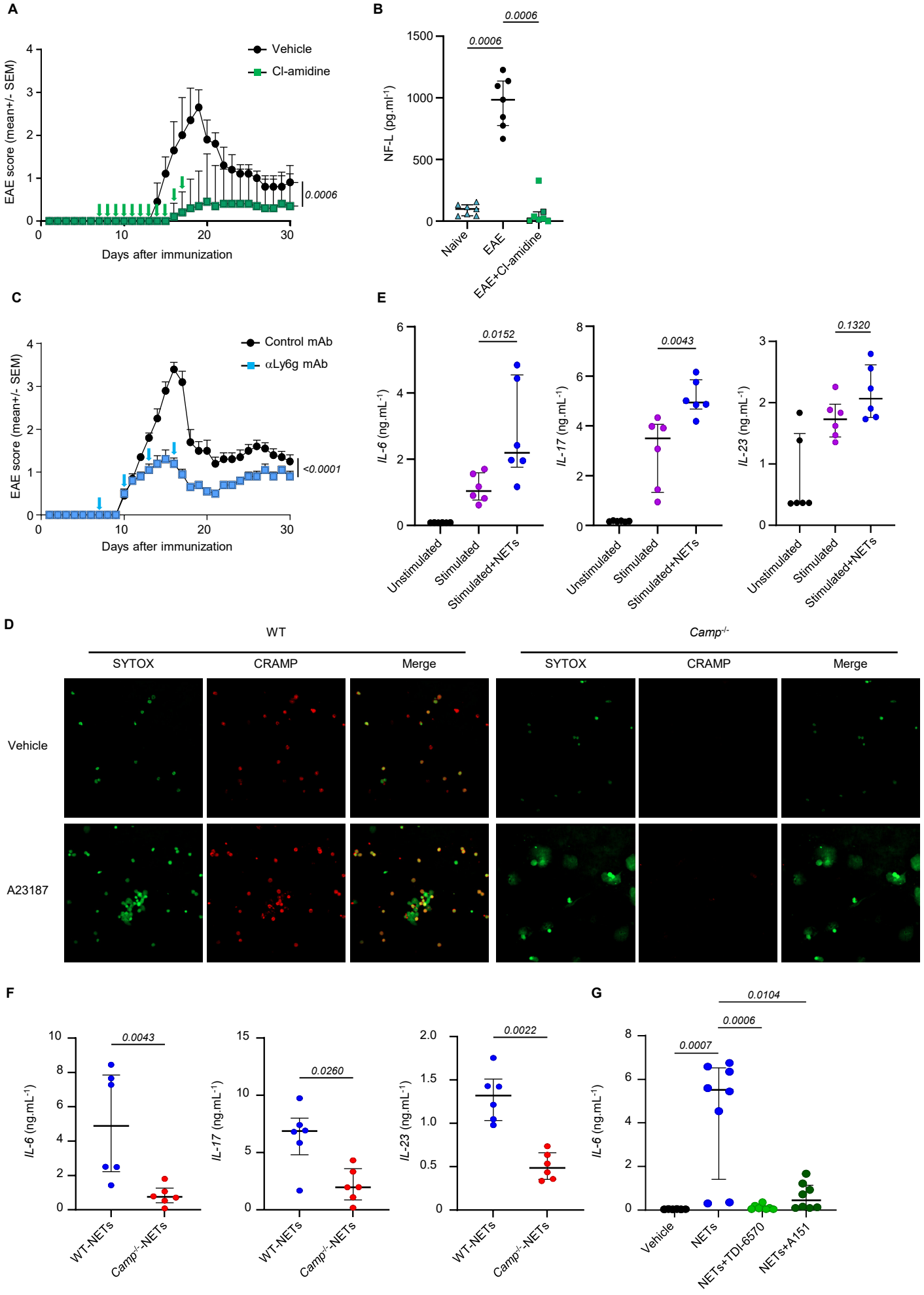
A
Vehicle
Cl-amidine
EAE score (mean+/- SEM)
Days after immunization
0.0006
B
0.0006
0.0006
NF-L (pg.ml-1)
Naive
EAE
EAE+Cl-amidine
C
Control mAb
αLy6g mAb
EAE score (mean+/- SEM)
Days after immunization
<0.0001
E
0.0152
0.0043
0.1320
IL-6 (ng.mL-1)
IL-17 (ng.mL-1)
IL-23 (ng.mL-1)
Unstimulated
Stimulated
Stimulated+NETs
D
WT
Camp-/-
SYTOX
CRAMP
Merge
Vehicle
A23187
F
0.0043
0.0260
0.0022
IL-6 (ng.mL-1)
IL-17 (ng.mL-1)
IL-23 (ng.mL-1)
WT-NETs
Camp-/--NETs
G
0.0104
0.0006
0.0007
IL-6 (ng.mL-1)
Vehicle
NETs
NETs+TDI-6570
NETs+A151

Figure 4 CRAMP from NETs favors encephalitogenic T cell response. (A, C) WT mice (n=10 mice/group from 2 independent experiments) were immunized with MOG35-55 to induce EAE. Mice were then treated s.c. with Cl-amidine daily from day 7 to 17 post EAE induction (A) or treated i.p. with neutrophil-depleting □Ly6G mAb or isotype control mAb every 3 days from day 7 to 17 post EAE induction (C). Clinical scores are shown (mean ± SEM). (B) NF-L protein levels were measured in the serum of Cl-amidine-treated mice 15 days after EAE induction. Data are the median +/− interquartile range of 7 independent mice per group from 3 independent experiments. (D) Neutrophils were isolated from bone marrow of tibia of WT and Camp-/- mice and activated with A23187 ionophore to induce NETs. Visualization of NETs was performed by confocal microscopy after DNA (SYTOXTM green) and CRAMP (red) staining. Data are representative of 3 independent experiments. (E, F) NETs were prepared from WT and Camp-/- mice as in (E) and added to splenocyte culture isolated from WT mice immunized with MOG35-55 10 days earlier. (G) BMDCs from WT mice were stimulated for 18 h with NETs. In some conditions, the cGAS inhibitor TDI-6570 or a multi-specific TLR9, AIM2 and cGAS antagonist ODN A151, were added to the culture 3 h before stimulation. Cytokine level in the supernatant was measured by multiplex ELISA. Data are the median +/− interquartile range of 6-8 independent wells from 3 independent experiments. Comparison between each group was performed using the non-parametric Mann-Whitney U-test, or Kruskal-Wallis test followed up by Dunn's post-test when more than 2 groups were compared. For evaluating differences between EAE scores over time, a two-way ANOVA with Tukey's multiple comparisons test was used.

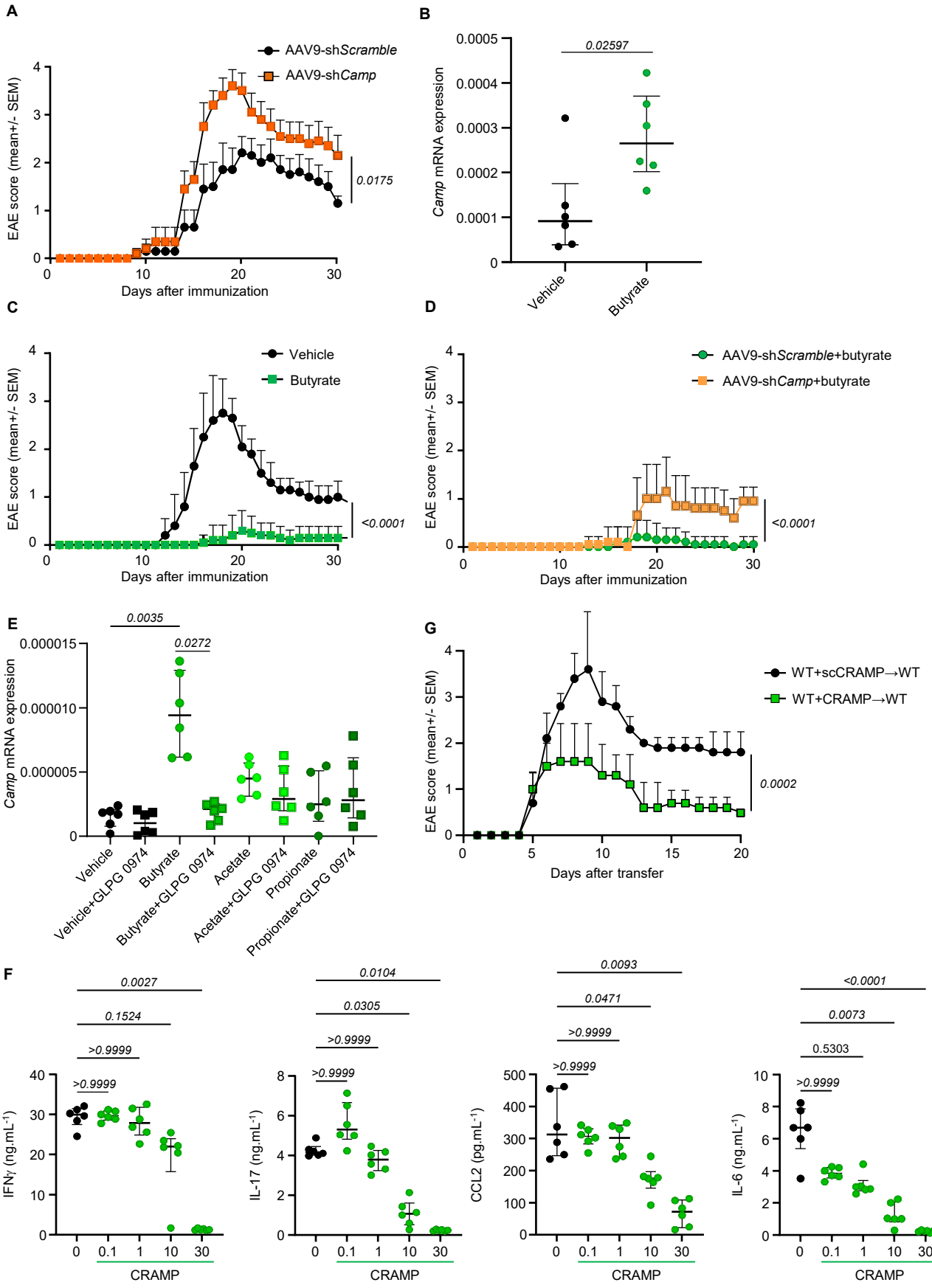
A
AAV9-shScramble
AAV9-shCamp
EAE score (mean+/- SEM)
Days after immunization
0.0175
B
0.02597
Camp mRNA expression
Vehicle
Butyrate
C
Vehicle
Butyrate
<0.0001
D
AAV9-shScramble+butyrate
AAV9-shCamp+butyrate
<0.0001
E
0.0035
0.0272
Camp mRNA expression
Vehicle
Vehicle+GLPG 0974
Butyrate
Butyrate+GLPG 0974
Acetate
Acetate+GLPG 0974
Propionate
Propionate+GLPG 0974
G
WT+scCRAMP→WT
WT+CRAMP→WT
0.0002
Days after transfer
F
IFNγ (ng.mL-1)
IL-17 (ng.mL-1)
CCL2 (pg.mL-1)
IL-6 (ng.mL-1)
CRAMP

Figure 5 CRAMP from neural cells dampens EAE. (A, C, D) WT mice were immunized with MOG35-55 to induce EAE. C57BL/6 mice were treated with i.t. injection of AAV9-shCamp or AAV9-shScramble at day -7 (A) or with p.o. butyrate from day 7 to day 30 (C) after EAE induction or with both (D). Clinical scores are shown (mean ± SEM). (n=12 mice per group from 3 independent experiments). (B) WT mice were treated in drinking water with sodium butyrate (10 g.L-1) for 7 days. Spinal cord was recovered, and Camp expression determined by RT-qPCR. Data are the median +/− interquartile range of 6 independent mice per group from 3 independent experiments. (E) Neuron NSC-34 cells were cultured for 24h in the presence of either butyrate, acetate or propionate analysis of Camp expression by RT-qPCR. In some conditions, the FFAR2/3 antagonist GLPG 0974 was added to the cells 2h before the SCFAs. Data are the median +/− interquartile range of 3 independent experiments. (F) Splenocytes were recovered 10 days after EAE induction in WT mice and cultured for 3 days with MOG35-55 in pro-Th17 conditions with growing doses of CRAMP1-39 (µg.mL-1). Cytokine level was measured in the supernatant by multiplex ELISA. Data are the median +/− interquartile range of 6 independent mice per group from 3 independent experiments. (G) Splenocytes were recovered 10 days after EAE induction in WT mice and were cultured for 3 days with MOG35-55 in pro-Th17 conditions with either CRAMP1-39 or scramble (sc) CRAMP1-39 (10 µg.mL-1) and transferred in WT mice. Clinical scores are shown (mean ± SEM) (n=12 mice/group; 3 independent experiments). Comparison between each group was performed using the non-parametric Mann-Whitney U-test, or Kruskal-Wallis test followed up by Dunn's post-test when more than 2 groups were compared. For evaluating differences between EAE scores over time, a two-way ANOVA with Tukey's multiple comparisons test was used.

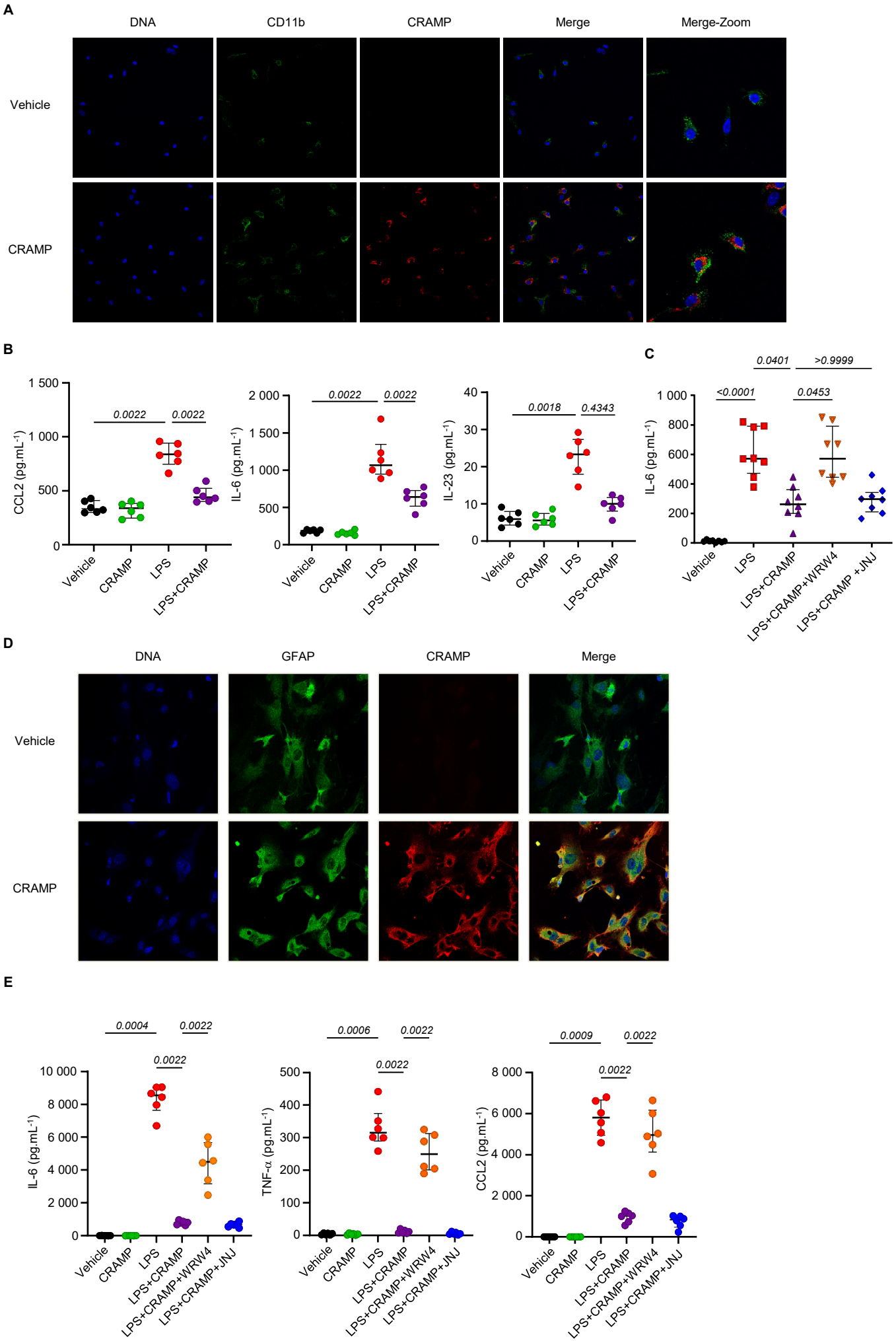
A
DNA
CD11b
CRAMP
Merge
Merge-Zoom
Vehicle
CRAMP
B
CCL2 (pg.mL-1)
1 500
1 000
500
0
0.0022
0.0022
IL-6 (pg.mL-1)
2 000
1 500
1 000
500
0
0.0022
0.0022
IL-23 (pg.mL-1)
40
30
20
10
0
0.0018
0.4343
Vehicle
CRAMP
LPS
LPS+CRAMP
C
IL-6 (pg.mL-1)
1 000
800
600
400
200
0
0.0401
>0.9999
<0.0001
0.0453
Vehicle
LPS
LPS+CRAMP
LPS+CRAMP+WRW4
LPS+CRAMP +JNJ
D
DNA
GFAP
CRAMP
Merge
Vehicle
CRAMP
E
IL-6 (pg.mL-1)
10 000
8 000
6 000
4 000
2 000
0
0.0004
0.0022
0.0022
TNF-α (pg.mL-1)
500
400
300
200
100
0
0.0006
0.0022
0.0022
CCL2 (pg.mL-1)
8 000
6 000
4 000
2 000
0
0.0009
0.0022
0.0022
Vehicle
CRAMP
LPS
LPS+CRAMP
LPS+CRAMP+WRW4
LPS+CRAMP+JNJ

Figure 6 CRAMP dampens microglia and astrocyte activation. (A) Microglia culture was prepared from Camp-/- mice and 10 µg.mL-1 of CRAMP or vehicle was added for 24h before staining for CD11b (green), CRAMP (red) and DNA (blue) and analysis by confocal microscopy. Data are representative of 3 independent experiments. (B−C) Microglia culture was prepared from WT mice and activated or not with LPS for 24 h before wash and addition of 10 µg.mL-1 CRAMP1-39 or vehicle for an additional 24h. In C, FPR2 antagonist WRW4 or P2X7R antagonist JNJ-47695567 was added 2h before CRAMP1-39 addition. Cytokine levels were measured in the supernatant by multiplex ELISA. Data are the median +/− interquartile range of 6-8 independent mice per group from 3 independent experiments. (D) Astrocyte culture was prepared from Camp-/- C57BL/6 mice and 10 µg.mL-1 CRAMP or vehicle was added for 24h before staining for GFAP (green), CRAMP (red) and DNA (blue) and analysis by confocal microscopy. Data are representative of 3 independent experiments. (E) Astrocyte cultures were prepared from WT mice and activated or not with LPS for 24h before wash and addition of 10 µg.mL-1 CRAMP1-39 or vehicle for an additional 24 h. The FPR2 antagonist WRW4 or P2X7R antagonist JNJ-47695567 was added 2 h before CRAMP1-39 addition. Cytokine levels were measured in the supernatant by multiplex ELISA. Data are the median +/− interquartile range of 6 independent mice per group from 3 independent experiments. Comparison between each group was performed using the non-parametric Mann-Whitney U-test, or Kruskal-Wallis test followed up by Dunn's post-test when more than 2 groups were compared.